Bralower, T.J., Premoli Silva, I., and Malone, M.J. (Eds.)
*Proceedings of the Ocean Drilling Program, Scientific Results* Volume 198

# 8. Evidence for Lysocline Shoaling at the Paleocene/Eocene Thermal Maximum on Shatsky Rise, Northwest Pacific[1]

Amanda B. Colosimo,[2] Timothy J. Bralower,[3]
and James C. Zachos[4]

## ABSTRACT

The Paleocene/Eocene Thermal Maximum (PETM) was a transient interval of global warming ~55 m.y. ago associated with transformation of ecosystems and changes in carbon cycling. The event was caused by the input of massive amounts of $CO_2$ or $CH_4$ to the ocean-atmosphere system. Rapid shoaling of the lysocline and calcite compensation depth (CCD) is a predicted response of $CO_2$ or $CH_4$ input; however, the extent of this shoaling is poorly constrained. Investigation of Ocean Drilling Program (ODP) Sites 1209–1212 at Shatsky Rise, which lies along a depth transect, suggests a minimum lysocline shoaling of ~500 m in the tropical Pacific Ocean during the PETM. The sites also show evidence of $CaCO_3$ dissolution within the sediment column, carbonate "burn-down" below the level of the carbon isotope excursion, and a predicted response to a rapid change in deepwater carbonate saturation. Close examination of several foraminiferal preservation proxies (i.e., fragmentation, benthic/planktonic foraminiferal ratios, coarse fraction, and $CaCO_3$ content) and observations of foraminifers reveal that increased fragmentation levels most reliably predict intervals with visually impoverished foraminiferal preservation as a result of dissolution. Low $CaCO_3$ content and high benthic/planktonic ratios also mirror intervals of poorest preservation.

[1]Colosimo, A.B, Bralower, T.J., and Zachos, J.C., 2006. Evidence for lysocline shoaling at the Paleocene/Eocene Thermal Maximum on Shatsky Rise, northwest Pacific. *In* Bralower, T.J., Premoli Silva, I., and Malone, M.J. (Eds.), *Proc. ODP, Sci. Results,* 198, 1–36 [Online]. Available from World Wide Web: <http://www-odp.tamu.edu/publications/198_SR/VOLUME/CHAPTERS/112.PDF>. [Cited YYYY-MM-DD]
[2]Department of Chemistry and Geology, Monroe Community College, 1000 East Henrietta Road, Rochester NY 14623, USA.
[3]Department of Geosciences, Pennsylvania State University, University Park PA 16802, USA. **bralower@geosc.psu.edu**
[4]Department of Earth Sciences, University of California, Santa Cruz CA 95064, USA.

Initial receipt: 8 March 2004
Acceptance: 8 September 2005
Web publication: 31 January 2006
Ms 198SR-112

# INTRODUCTION

The Paleocene/Eocene Thermal Maximum (PETM) was an interval of rapid global warming ~55 m.y. ago at the Paleocene/Eocene (P/E) boundary. The event is associated with an array of faunal and floral changes: the largest deep sea foraminiferal extinction event in the last 90 m.y., rapid planktonic foraminiferal diversification, appearance of several land mammal groups, transient turnover in nannoplankton assemblages, and a bloom of the shallow-water dinoflagellate genus *Apectodinium* (e.g., Maas et al., 1995; Kelly et al., 1998; Thomas, 1998; Crouch et al., 2001; Bralower, 2002).

Associated with these biotic changes is a negative carbon isotope excursion (CIE) of –2‰ to –3‰ in marine and terrestrial reservoirs (e.g., Kennett and Stott, 1991; Koch et al., 1992; Bains et al., 1999). The magnitude, global nature, and abrupt onset ($<10^4$ yr) of the CIE require rapid transfer of a massive amount of isotopically light carbon to the ocean-atmosphere system (e.g., Dickens et al., 1995). Several sources for this light carbon have been proposed including volcanic outgassing (e.g., Eldholm and Thomas, 1993), rapid burning of terrestrial organic matter (Kurtz et al., 2003), impact of a comet (Kent et al., 2003), and massive dissociation of methane hydrates along continental margins (e.g., Dickens et al., 1995, 1997; Katz et al., 1999; Svenson et al., 2004). Because the reservoir of methane hydrate in continental margin sediments is extremely large and their carbon isotopic composition is highly depleted ($\delta^{13}C$ value of approximately –60‰) (e.g., Kvenvolden, 1993), hydrate dissociation most readily explains the magnitude and rate of onset of the CIE (e.g., Dickens et al., 1997).

One of the main effects of introduction of a large amount of $CH_4$ or $CO_2$ into the ocean-atmosphere system is a rapid shoaling of the lysocline, the depth range of increased $CaCO_3$ solubility, and the calcite compensation depth (CCD), the depth below which all $CaCO_3$ is dissolved (e.g., Dickens et al., 1997). Ample evidence exists for shoaling of both surfaces in widespread locations (e.g., Lu and Keller, 1993; Schmitz et al., 1996; Thomas and Shackleton, 1996; Bralower et al., 1997; Thomas et al., 1999; Erbacher, Mosher, Malone, et al., 2004; Zachos, Kroon, Blum, et al., 2004; Zachos et al., 2005). The source of carbon, and especially whether it is introduced in the deep ocean or atmosphere, will greatly affect lysocline and CCD behavior (e.g., Dickens et al., 1997; Dickens, 2000). For example, if $CH_4$ reached the atmosphere prior to oxidation or if $CO_2$ was not completely dissolved in the deep ocean (e.g., Dickens et al., 1997; Dickens, 2000; Thomas et al., 2002), less shoaling would occur than if oxidation of $CH_4$ or dissolution of $CO_2$ occurred entirely in the deep ocean. The extent of shoaling would vary between basins largely depending on the source of the $CH_4$ or $CO_2$ and deepwater circulation patterns. Thus, the behavior of the lysocline and CCD in different parts of the ocean can be used to constrain the source of carbon during the PETM and its distribution through the atmosphere and oceans (Zachos et al., 2005).

The timing and scale of carbon sequestration can also be constrained from the lysocline and CCD. As $CO_2$ is removed from the system, primarily through weathering of silicates and organic carbon burial, the concentration of bicarbonate begins to rise, and the lysocline and CCD deepen, resulting in a transient supersaturation of bicarbonate in the deep sea. In theory, the lysocline may overshoot its preexcursion level during this recovery period (Dickens et al., 1997).

Global warming is another anticipated outcome of input of a massive amount of $CH_4$ or $CO_2$ to the ocean-atmosphere system. Stable isotope and trace element data suggest that sea-surface temperatures in the PETM increased by ~8°C at high latitudes and ~5°C at low latitudes and in deep waters (e.g., Kennett and Stott, 1991; Bralower et al., 1995; Zachos et al., 2003). However, several PETM stable isotope records have been obscured by recrystallization due to burial, which prohibits paleotemperature estimates (Bralower et al., 1997; Norris, Kroon, Klaus, et al., 1998). In addition, lysocline and CCD fluctuations could result in partial dissolution of, and overgrowth on, foraminiferal tests, altering isotope signatures. Rapid lysocline and CCD shoaling would result in large-scale carbonate dissolution, increasing the concentration of bicarbonate in pore waters. As the lysocline and CCD recover, supersaturation of bicarbonate at the seafloor would enhance precipitation of secondary calcite. Constraining the changes in the lysocline and CCD would help interpretation of stable isotope and trace metal ratios of altered PETM foraminifers.

The extent and rate of lysocline and CCD shoaling during the PETM can be approximated in closely spaced sites along a depth transect in middle to lower bathyal water depths using visual observations of foraminiferal preservation and a suite of other preservational proxies. One of the goals of Ocean Drilling Program (ODP) Leg 198 to Shatsky Rise, a large igneous province in the western Pacific Ocean (Fig. **F1**), was to obtain such a depth transect of PETM sites (Bralower, Premoli Silva, Malone, et al., 2002), one that would also complement a similar depth transect planned for the Atlantic (Leg 208) (Zachos, Kroon, Blum, et al., 2004). The PETM was recovered at relatively shallow burial depths at four sites on the Southern High of Shatsky Rise (Sites 1209–1212) (Tables **T1, T2, T3, T4**), ranging from 2387 to 2907 m water depth. In these sections, the PETM interval corresponds to an 8- to 23-cm-thick layer of clayey nannofossil ooze with a sharp base and a gradational upper contact (Fig. **F2**). An extremely thin (1 mm) dark brown clay seam lies at the base of this contact in several locations. At the deepest site drilled on Shatsky Rise (Site 1208 on the Central High; 3346 m water depth), the PETM interval is highly condensed (<3 cm), lies in a dark claystone with few nannofossils and almost no foraminifers, and was clearly close to the CCD before, during, and after the event. At all sites, the CIE was identified using bulk carbon isotope measurements. Plate reconstructions and benthic foraminiferal assemblages suggest that Sites 1209–1212 were located at ~20°N and ~2400–2900 m water depth during the PETM, similar to their present water depths (Bralower et al., 2002).

In this investigation, potential carbonate preservational proxies were evaluated in sections from the Shatsky Rise depth transect and used to interpret the response of the tropical Pacific lysocline during the PETM.

## METHODOLOGY

Samples from Sites 1209–1212 were obtained from continuous U-channels through the PETM. Samples of ~1 $cm^3$ were rinsed in distilled water, dried for 24 hr, weighed, washed with buffered water (pH ~10) and 5% Calgon solution, then disaggregated on a gyratory table for ~12 hr. Samples were then washed through 38- and 63-µm sieves, dried at ~40°C for 24 hr, and reweighed. Since the >38- and >63-µm fractions have very similar trends at all four sites (Fig. **F3**), the >63-µm fraction is referred to as the coarse fraction.

Detailed counts were performed to characterize preservation. Samples were dry-sieved to isolate specimens >125 µm, poured onto a picking tray, and observed using a binocular light microscope. The first ~300 grains encountered in traverses of the picking tray were counted per sample. Grains were identified as whole planktonic foraminifers, fragmented planktonic foraminifers, benthic foraminifers, pyrite, or fish debris. Fragmented foraminifers include specimens showing notable deterioration, including missing chambers and substantial breakage. Three samples were recounted to ensure consistency; reproducibility is ±10% (Fig. F4). Calcium carbonate content for each site was measured from dried bulk samples using a $CO_2$ coulometer. External precision based on replicate measurements is ±2%.

Foraminiferal preservation was documented using a scanning electron microscope (SEM) for comparison with other preservational proxies. Foraminifers used for preservational analyses were ultrasonified for ~5 s to remove nannofossils and clay, resieved, and dried. Representative specimens were mounted on SEM stubs, broken with a metal pick, and photographed to assess chamber infilling and secondary calcite overgrowth and reprecipitation. We illustrate the range of foraminiferal preservation observed in several samples (Pls. P1, P2, P3, P4, P5, P6, P7).

Stable isotope analyses were carried out on 100–500 µg of freeze-dried bulk sample using Autocarb common acid bath systems coupled to either a PRISM or OPTIMA mass spectrometer. All values are reported relative to Vienna Peedee belemnite as calibrated by replicate analyses of National Bureau of Standards (NBS)-19 and in-house standard Carrara marble.

# RESULTS

## Stable Isotope Ratios

The CIE is recorded by bulk sediment at each site. At Sites 1209, 1210, 1211, and 1212, the magnitude of the excursion is ~2.5‰. The negative excursion covers an interval of several centimeters at and above the lithologic contact. The return to stable values, or the "recovery interval," shows a depth-dependent pattern with the recovery spanning ~80 cm at Site 1209 and ~50 cm at Site 1212. At Site 1211 the recovery is clearly truncated.

As the onset of the CIE at the base of the PETM is a "golden spike" that formally defines the P/E boundary; trends in all other records are described relative to this horizon (0 cm).

## Weight Percent Coarse Fraction

Weight percent coarse fraction trends vary significantly between the four sites despite their relative proximity. At Site 1209, coarse fraction increases at the base of the CIE (0 cm), reaches a maximum between 5 and 11 cm above the CIE, and then steadily decreases to background levels at about +22 cm (Fig. F5). This is similar to the coarse fraction at Site 1210, which begins to increase at 0 cm, reaches a maximum at +2 cm, then declines to background levels at +14 cm (Fig. F6).

The abrupt increases in coarse fraction at Sites 1209 and 1210 are not observed at the deeper Sites 1212 and 1211. Coarse fraction at Site 1212 is relatively low until about +2 cm, where it steadily increases and re-

F4. Replicant counts histogram, p. 20.

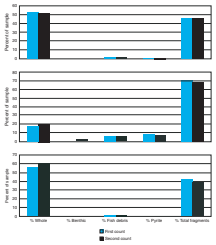

P1. Planktonic foraminifers, +1 cm, p. 29.

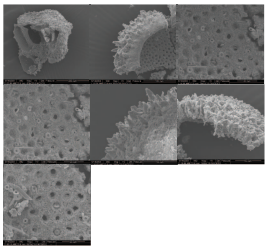

P2. Planktonic foraminifers, +2 cm, p. 30.

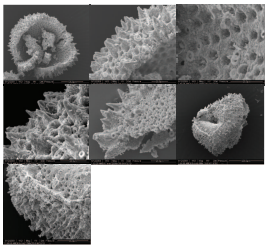

P3. Planktonic foraminifers, +3 cm, p. 31.

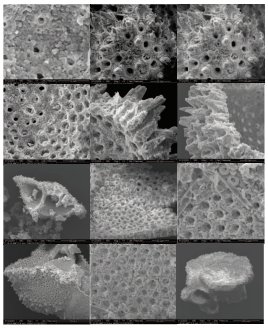

P4. Planktonic foraminifers, +4 cm, p. 32.

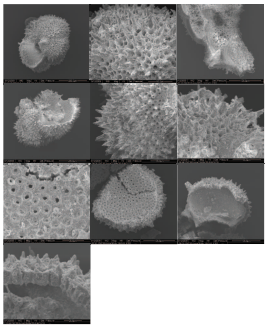

mains high through +16 cm (Fig. F7). At Site 1211, coarse fraction decreases slightly beginning just below 0 cm, then increases at +4 cm (Fig. F8).

## Weight Percent Calcium Carbonate

At Site 1209, $CaCO_3$ decreases from 97 wt% at –3 cm to 86 wt% at +2 cm and then increases in an irregular fashion to 97 wt% at +17 cm (Fig. F5). At Site 1210, $CaCO_3$ decreases from 93 to 86 wt% from –3 to 0 cm, remains low (<91 wt%) until +10 cm and then remains relatively constant at >90 wt% to +92 cm. Samples with decreased $CaCO_3$ at Sites 1209 and 1210 correspond to the interval with elevated coarse fraction (Figs. F5, F6).

$CaCO_3$ decreases from 98 to 83 wt% at –1 cm at Site 1212 and remains mostly <90 wt% up to +10 cm, where it increases to >95 wt% (Fig. F7). $CaCO_3$ is more variable at Site 1211 (Fig. F8). There is a general decline in $CaCO_3$ content from >95 wt% at –4 cm to 70 wt% at +3 cm. $CaCO_3$ content increases at +3 cm from 70 to 92 wt%. Lowest recorded $CaCO_3$ occurs at the deepest site, Site 1211.

## Foraminiferal Fragmentation

Foraminiferal fragmentation is the percentage of foraminifers that are broken in each sample. At Site 1209, fragmentation increases from 33% at –4 cm to 63% at 0 cm and then decreases to 27% at +5 cm (Fig. F5). At Site 1210, fragmentation is also highest (77%) at the base of the CIE but remains above 40% from –3 cm to +6 cm (Fig. F6). At Site 1212, fragmentation begins to increase from 10%–15% below –2 cm to 25% at –1 cm, peaks (70%) at +2 cm and then decreases to ~35% above +5 cm (Fig. F7). Fragmentation begins to increase at 0 cm at Site 1211, peaks (66%) at +3 cm (Fig. F8) and then decreases to ~30% above +5 cm.

At the two sites with records that extend well above the dissolution horizon (Sites 1209 and 1210), fragmentation drops to levels below pre-excursion values.

## Benthic/Planktonic Ratios

A high benthic/planktonic foraminiferal ratio (B/P) has often been used as an indicator of dissolution (e.g., Corliss and Honjo, 1981). In all examined Shatsky Rise samples, benthic foraminifers are relatively rare. At Site 1209, the highest B/P (0.04) was found at 0 cm (Fig. F5). The highest B/P at Site 1210 (0.11) was at –12 cm, with a second maximum at –1 cm (0.09) (Fig. F6). The B/P is >0.02 from 0 to +1 cm at Site 1212 (Fig. F7). At the deepest site, Site 1211, the B/P is highest (0.06) at +2 cm (Fig. F8).

## Percent Pyrite

Pyrite was observed as coatings on foraminifers and as discrete particles. At Site 1209, pyrite content peaked (3%) at the CIE onset (Fig. F5). At Site 1210, pyrite abundance increased in the interval below the CIE and peaked at the onset (9%) (Fig. F6). Very little pyrite was recovered above base of the CIE at Sites 1209 and 1210. At Site 1212, pyrite abundance increased significantly at the CIE onset and reached a maximum at +1 cm (8%) (Fig. F7). At Site 1211, significant pyrite was confined to

P5. Planktonic foraminifers, +5 cm, p. 33.

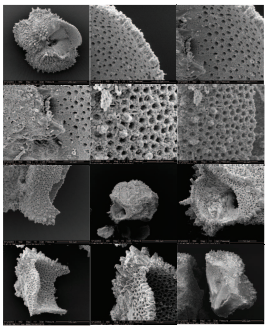

P6. Planktonic foraminifers, +6 cm, p. 34.

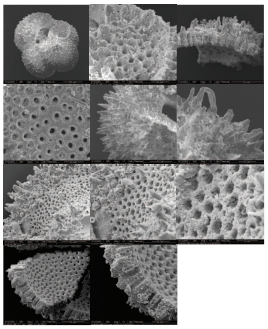

P7. Planktonic foraminifers, +7 cm, p. 35.

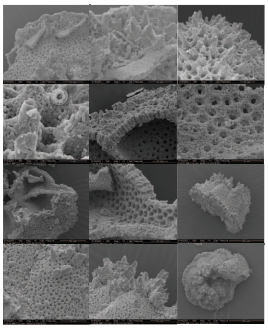

F5. Sample data, Hole 1209B, p. 21.

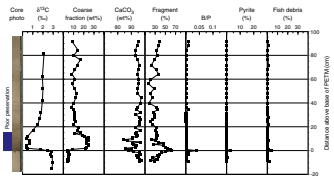

samples from +1 to +3 cm, and maximum content (28%) occurred at +2 cm (Fig. F8). Pyrite abundance steadily increases from the shallowest to deepest sites.

### Percent Fish Debris

Fish debris includes fish teeth, scales, and bones. At Site 1209, maximum fish debris (4%) was recovered at the onset of the CIE coincident with the maxima in fragmentation, pyrite, and B/P ratio (Fig. F5). The peak in fish debris at Site 1210 extends from –4 to 0 cm and is centered (17%) at –2 cm (Fig. F6). At Site 1212, the peak in fish debris (40%) lies at +1 cm (Fig. F7). At Site 1211, fish debris is concentrated between +1 and +3 cm, with a peak (35%) at +2 cm (Fig. F8). The two deeper sites have a much higher abundance of fish debris than the two shallower sites.

### Preservational Survey

An extensive survey of pore infilling and secondary calcite precipitation on foraminifers was conducted. Trends in visual foraminiferal preservation were correlated to the quantitative variables. Extensive micrographs documenting foraminiferal preservation can be found in Colosimo (2004); we present a summary of micrographs showing preservation across the base of the PETM in Hole 1209B in Plates P1, P2, P3, P4, P5, P6, and P7. We indicate the interval of poorest preservation in Figures F5, F6, F7, and F8.

Preservation is moderate before and after the PETM interval at Site 1209 but deteriorates at 0 cm and remains poor until +15 cm (Pls. P1, P2, P3, P4, P5, P6, P7; Fig. F5). Blocky secondary calcite is observed throughout the entire interval of poorest preservation with infilling of chambers and extensive overgrowth on muricae and walls. At Site 1210, foraminiferal preservation is moderate below and above the lithologic contact. Preservation deteriorates abruptly at 0 cm and remains poor until about +10 cm (Fig. F6). In this interval, extensive pore infilling with secondary calcite was observed. Euhedral calcite blades 5–10 µm long have also been observed on chamber walls in the interval of poorest preservation.

Foraminifers are generally more overgrown with secondary calcite at Site 1212 than at Site 1210. Preservation deteriorates significantly at the lithologic change and remains poor for much of the studied record (Fig. F7). Euhedral calcite blades were observed on chamber walls throughout this entire studied section. Less calcite overgrowth is observed on foraminifers at Site 1211, although preservation is poor from 0 to +5 cm (Fig. F8).

## DISCUSSION

### Proxy Validation

Several different types of data have been used as indicators of foraminiferal preservation, including $CaCO_3$ content, B/P ratio, coarse fraction, and fragmentation (e.g., Arrhenius, 1952; Corliss and Honjo, 1981; Thierstein and Roth, 1991; Haug and Tiedemann, 1998). Close examination of these data in the PETM interval at Shatsky Rise and comparison with visual preservation will help establish the most reli-

F6. Sample data, Hole 1210B, p. 22.

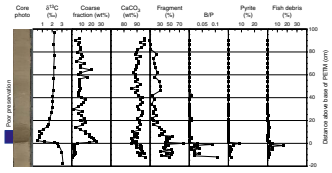

F7. Sample data, Hole 1212B, p. 23.

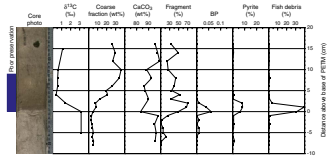

F8. Sample data, Hole 1211C, p. 24.

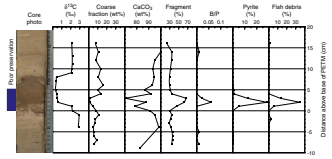

able proxy, or combination of proxies, for preservation. Lithology and the CIE allow precise correlation of data between sites. The onset of the PETM is marked by the abrupt onset of the bulk carbonate $\delta^{13}C$ excursion which lies at or just below a sharp lithologic contact between more carbonate rich ooze overlying clay-rich ooze (Figs. **F5, F6, F7, F8**). In the upper part of the PETM interval, the clay-rich ooze gradually becomes more carbonate rich and $\delta^{13}C$ values of bulk carbonate gradually increase. Whereas no pristine foraminiferal preservation is observed in the PETM interval on Shatsky Rise, there is an abrupt deterioration in preservation at the basal lithologic contact and the base of the CIE at each site. This change includes a substantial increase in pore infilling and sparry calcite in foraminiferal chambers and on muricae (Pls. **P1, P2, P3, P4, P5, P6, P7**). The quality of preservation recovers gradually above the PETM with a steady decrease in secondary calcite and pore infilling. Preservation generally deteriorates with water depth, with the deepest location (Site 1211) showing evidence for stronger dissolution, indicating more corrosive waters than in the shallower sites. In the interval of poorest preservation at all sites, euhedral calcite blades ~10 Mm in length and blocky rhombs of calcite indicate that initial dissolution led to at least temporary supersaturation of $CaCO_3$ in pore waters.

Dissolution results in enlarged pores and breakage of foraminiferal tests (e.g., Broecker and Peng, 1982). Changes in fragmentation mirror the poorest preservation in samples near the basal lithologic contact at each site and the overlying gradual recovery of preservation. Although maximum fragmentation occurs at or just above the onset of the CIE and lithologic contact, fragmentation begins to increase slightly *below* this level at Sites 1209, 1210, and 1212. The sharp lithologic contact indicates little mixing and thus shows that dissolution of foraminifers occurred during early burial.

Fragmentation is typically high at each site for several centimeters above the lithologic contact, corresponding to the interval of poor preservation and greatest dissolution. The thickness of the fragmentation interval decreases with depth. At Site 1209 (2387 meters below sea level [mbsl]), fragmentation is high over an 8-cm interval. Fragmentation is elevated over 7 cm at Site 1210 (2573 mbsl) and 5 cm at Sites 1212 (2681 mbsl) and 1211 (2907 mbsl) (Figs. **F5, F6, F7, F8**). Background fragmentation levels also increase with depth, ranging from ~20% at Sites 1209 and 1210 to ~30% at Sites 1211 and 1212 (Figs. **F5, F6, F7, F8**). This also indicates increased dissolution with depth.

Calcium carbonate content has often been used as a proxy for changes in preservation during burial diagenesis (e.g., Arrhenius, 1952). Previous work (Thierstein and Roth, 1991) showed that nannofossils and foraminifers in samples with $CaCO_3$ contents between 60 and 80 wt% are characterized by little diagenetic overgrowth or dissolution. Samples containing <60 wt% $CaCO_3$ generally show evidence for dissolution and those >80 wt% often show evidence for secondary calcite overgrowth. Shatsky Rise PETM $CaCO_3$ contents range from 70 to >95 wt%, which under normal circumstances would cause minor overgrowth during burial. However, predicted PETM $CO_2$ input should result in a rapid increase in carbonate solubility at the seafloor with corresponding changes in $CaCO_3$. At all four sites, significant decreases in $CaCO_3$ content mirror intervals of poor preservation, suggesting dissolution as the main control on $CaCO_3$ values (Figs. **F5, F6, F7, F8**). At Sites 1209, 1210, 1212, and 1211, $CaCO_3$ content decreases by 10% over 4 cm, 7% over 3 cm, 15% over 3 cm, and ~25% over 4 cm, respec-

tively. Although the PETM was a transient event, carbonate production in surface waters likely responded to warming and ocean circulation changes (Thomas et al., 1999; Bralower, 2002; Stoll and Bains, 2003). Consequently, decreased $CaCO_3$ content may also be a partial result of decreased surface water productivity.

Coarse fraction has often been interpreted as a proxy for foraminiferal preservation (e.g., Haug and Tiedemann, 1998). Increases in coarse fraction are generally interpreted as indicative of better preservation, as foraminifers are thought to be more susceptible to dissolution than nannoplankton (e.g., Schlanger and Douglas, 1974). At Sites 1209 and 1210, however, highest coarse fraction occurs in intervals of poorest visual preservation (Figs. **F5, F6**). At Site 1212, coarse fraction increases 2–3 cm above the basal contact, within the interval of poor preservation (Fig. **F7**). Only Site 1211 shows a decrease in coarse fraction in the interval of poor preservation (Fig. **F8**). Because coarse fraction increases with dissolution at three of the four sites, it is unreliable as a proxy for preservation. High coarse fraction at Sites 1209, 1210, and 1212 may be the result of changing environmental variables such as productivity.

Benthic foraminifers are generally more resistant to dissolution than planktonic foraminifers (e.g., Lipps, 1973; Thomas and Shackleton, 1996; Thomas 1998), so increases in B/P may also be indicative of dissolution. B/P ratios are consistent with preservational trends at Sites 1209, 1211, and 1212 (Figs. **F5, F7, F8**), but the B/P maximum at Site 1210 does not correspond to any visual change in preservation (Fig. **F6**). The abrupt B/P peaks at Sites 1209, 1211, and 1212 correspond to the most extreme dissolution intervals and fail to capture the extent of the interval of poor preservation. Benthic foraminifers were relatively rare (<6%) in all samples. Thus, counting finer-size fractions (>38 or >63 µm) may have recovered more benthic foraminifers, providing more robust and detailed B/P curves.

Percent fish debris appears to be a sensitive indicator of dissolution. At all sites, fish debris peaks at the same depth as fragmentation maxima (Figs. **F5, F6, F7, F8**). Assuming that fish debris is deposited at a constant rate, seafloor dissolution should result in increased concentrations. Percent fish debris also generally increases with depth: maximum fish debris is 4% at Site 1209, 17% at Site 1210, 40% at Site 1212, and 36% at Site 1211 (Figs. **F5, F6, F7, F8**). This trend indicates higher apparent sedimentation rates at Sites 1209 and 1210, as more carbonate is dissolved in increasingly corrosive bottom waters at the deeper sites. Abrupt short-term increases in pyrite abundance also occur near the basal lithologic contact. Higher amounts of pyrite coincide with maximum values of fragmentation (Figs. **F5, F6, F7, F8**).

Comparison of intervals of poor visual preservation with all of the possible preservational proxies suggests that foraminiferal fragmentation is the most reliable indicator of preservation in the PETM intervals recovered on Shatsky Rise. Visual inspection suggests that poor preservation corresponds to intervals of lower $CaCO_3$ content. B/P counts also faithfully record intervals of poorest preservation, but too few benthic foraminifers were recovered to identify the complete interval of increased dissolution. Coarse fraction percent responds to dissolution as expected only at the deepest location, Site 1211.

## Theoretical Lysocline Shoaling Model

Regardless of origin, input of massive amounts of $CO_2$ or $CH_4$ into the ocean-atmosphere system would lead to a marked shoaling of the lysocline and CCD (e.g., Dickens et al., 1997). The response of the lysocline and CCD is sensitive to the location of carbon input at the onset of the PETM and its distribution through the ocean and atmosphere (e.g., Dickens, 1997; Zachos et al., 2005). In the case of a methane hydrate source, the site of oxidation of $CH_4$ to $CO_2$ is critical (Dickens, 2000). If the carbon source is oceanic (either from methane hydrate or submarine volcanism), the response of the lysocline and CCD can help determine whether, and how rapidly, the carbon entered the atmosphere as well as how it was mixed through the ocean basins (e.g., Dickens, 2000, 2001). For example, if methane hydrate is the source of carbon and oxidation took place in the Atlantic, then the lysocline would be expected to shoal more dramatically in that ocean than in the Pacific (Zachos et al., 2005). A similar result would occur if thermohaline circulation patterns during the PETM were similar to present and carbon rapidly entered the atmosphere from the ocean or originated in the atmosphere (i.e., from an extraterrestrial source or subaerial volcanism). However, if methane hydrate was input and oxidized in other locations including the Pacific, Indian, or Southern Oceans, or if these oceans were deepwater source regions (e.g., Thomas et al., 2003; Svenson et al., 2004), then they would be expected to show a more marked response. Changes in the efficiency of the biological pump during the PETM (e.g., Bains et al., 1999; Crouch et al., 2001; Bralower, 2002) also would have led to variations in the lysocline and the CCD. For example, increased supply of carbonate would tend to lead to a deepening of both levels.

A variety of evidence, including single specimen foraminiferal isotope data, indicates that a large portion of the $CO_2$ or $CH_4$ that forced the PETM was rapidly released into the atmosphere (e.g., Dickens, 2000; Thomas et al., 2002). However, the early timing of the decrease in $CaCO_3$ relative to biotic signals at ODP Site 690 suggests that a significant part of the $CO_2$, possibly derived from the oxidation of $CH_4$, remained in oceanic deep waters (Thomas et al., 2002). This conclusion assumes that at least part of the observed decrease in $CaCO_3$ was a result of dissolution and not a change in productivity.

A change in the depth of the lysocline can be identified by a sharp decrease in carbonate content or a deterioration of carbonate preservation (i.e., increased fragmentation). The CCD level can be identified by the near or complete absence of carbonate in sediments. Sediments from the PETM interval at Atlantic and Caribbean Deep Sea Drilling Project and ODP sites, and in Tethyan land sections, suggest a rapid, marked shoaling of the lysocline at the onset of the PETM. In some cases, the absence of $CaCO_3$ suggests these sites lay below the CCD during the early part of the event (e.g., Canudo et al., 1995; Thomas and Shackleton, 1996; Bralower et al., 1997; Thomas, 1998; Thomas et al., 1999; Erbacher, Mosher, Malone, et al., 2004; Zachos et al., 2005). At Sites 690 and 738 in the Atlantic and Indian Ocean sectors of the Southern Ocean, respectively, the base of the PETM shows a less significant decrease in carbonate content (Thomas et al., 1999; C. Kelly, pers. comm., 2005). Little change in foraminiferal preservation occurs at Site 690 (Thomas et al., 2002), whereas dissolution increases at Site 738 (Lu and Keller, 1993).

Little information about the Pacific lysocline is available, largely because the PETM was either incompletely recovered (Site 865) (Bralower et al., 1995) or not recovered (i.e., during previous legs on Shatsky Rise), although Dickens (2000) interpreted the response of the lysocline in this ocean to be less than in the Atlantic. Background fragmentation levels (20%–30%) measured as a part of this investigation suggest that at least the deepest Shatsky Rise site investigated (Site 1211) was located in the upper range of the lysocline prior to the PETM and that all sites were within the lysocline during the event (fragmentation >40%).

The input of $CO_2$, possibly as a result of $CH_4$ oxidation, would result in increased dissolution of $CaCO_3$, especially in deeper water masses where $CO_2$ concentrations are elevated and $CaCO_3$ content is lower. This would result in a shoaling of the lysocline and CCD, as $CaCO_3$ would become soluble at increasingly shallower depths. As a result, foraminiferal fragmentation would increase and sedimentation rate decrease. Maximum pyrite, fish debris, and fragmentation were observed only in samples ±3 cm from the lithologic contact at all sites, consistent with a geologically instantaneous event, such as massive dissociation of methane hydrates.

If the dissolution rate of $CaCO_3$ exceeded the rain rate, foraminifers in the upper centimeters of the sediment column would dissolve, a concept referred to as carbonate "burn-down." Evidence for burn-down includes increased fragmentation and decreased $CaCO_3$ values below the basal PETM lithologic contact at Sites 1209, 1210, and 1212 (Figs. **F5, F6, F7**). Decreased $CaCO_3$ below the onset of the PETM has been noted at other PETM sites (Site 690 [Thomas and Shackleton, 1996] and the Leg 208 depth transect [Zachos et al., 2005]), but never with supporting visual observations and fragmentation data. Whereas burn-down has been predicted from models (Walker and Kasting, 1992; Dickens et al., 1997), the extent of such burn-down has not been previously constrained in a PETM section.

Increased $CO_2$ in deep waters in the vicinity of Shatsky Rise would cause the lysocline to shoal and increase saturation of $Ca^{2+}$ and $HCO_3^-$ in sediment pore waters. This would lead to secondary precipitation of $CaCO_3$ on foraminifers (Pls. **P1, P2, P3, P4, P5, P6, P7**) including overgrowth on walls and muricae and separate euhedral calcite blades in PETM sections, indicating at least temporary supersaturation of pore water $CaCO_3$ (aq.). There is no evidence in any of the preservational proxies that Sites 1209–1212 were situated below the CCD during the PETM. It is impossible to rule out, however, that the CCD shoaled above this depth range for a very short interval at the onset of the event (for example, ~1–2 k.y.), but leaving no substantial clay layer due to bioturbation. The magnitude of the bulk carbon isotope excursion at Shatsky Rise is smaller than that recorded at the shallowest of the Walvis Ridge sites (Site 1263), which would be consistent with a period of nondeposition of carbonate and truncation of the CIE at Shatsky Rise. Site 1208 on the Central High (3346 m) was clearly situated close to, but not below, the CCD during the PETM as there are no foraminifers in PETM sediments and only the most robust nannofossils are preserved (**Bown,** this volume).

We can obtain a minimum estimate for the amount of lysocline shoaling assuming that the deepest location on the Southern High (Site 1211; 2907 m) was located near the upper lysocline prior to the PETM. Our data show that even the shallowest location (Site 1209; 2387 m) lay below the lysocline at the peak of the PETM. Thus, a minimum estimate

for the extent of lysocline shoaling is ~520 m. This is significantly higher than an estimate for the Pacific (~250 m) from a model run in which $CH_4$ is oxidized in the Atlantic (Dickens et al., 1997; Dickens 2000) but similar to a run where $CH_4$ is oxidized in the deep Pacific Ocean (~600 m of shoaling), which is unlikely given the CCD shoaling in the Atlantic. Leg 199 in the equatorial Pacific recovered the PETM at Sites 1220 and 1221 (3.0 and 3.5 km paleodepth), and the cores from this interval show a sharp decrease in carbonate to very low values (Lyle, Wilson, Janecek, et al., 2003). The greater depth of the Leg 199 sites compared to those studied on Shatsky Rise is consistent with the evidence for increased dissolution and suggests a rapid shoaling of the CCD in this location (Lyle, Wilson, Janecek, et al., 2003).

Although the data presented here are most consistent with results from model runs in which $CH_4$ (and by inference, $CO_2$) is input directly into the deep Pacific, we do not conclude that this was the case. Atlantic PETM sections show evidence for more significant shoaling of the lysocline, and many sites at similar depths to those studied here were situated below the CCD during the early stages of the event (Dickens, 2000; Zachos et al., 2005). In particular, a depth transect on Walvis Ridge in the South Atlantic indicates at least 2 km shoaling of the CCD over 10 k.y. at the onset of the PETM (Zachos et al., 2005). Our results suggest that the models themselves may not adequately simulate the oceans or, more likely, that the amount of $CO_2$ input was far greater than assumed.

## Significance of Pyrite and the Benthic Foraminiferal Extinction

The benthic foraminiferal extinction (BFE) at the PETM was the largest extinction event in this group in the last 90 m.y. (Thomas, 1998). Suggested causes of the BFE include dissolution of benthic tests or lack of food (Thomas and Shackleton, 1996; Thomas, 1998; Thomas et al., 2000). Depleted oxygen levels in deep waters resulting from increased deep-sea temperatures, oxidation of $CH_4$ in the water column, locally or regionally increased productivity, or a combination of these factors is a possible cause of the BFE (e.g., Boersma et al., 1998; Thomas, 1998). Deepwater dissolved oxygen levels are difficult to determine but are essential to understanding the faunal response to events during the PETM. Abundance of pyrite can suggest $O_2$ depletion, especially in regions of high productivity where the rapid flux of organic matter rapidly consumes deepwater $O_2$ (e.g., Berner, 1977; Lerman, 1979; Müller and Suess, 1979; de Baar and de Jong, 2001). Independent evidence for low $O_2$ includes lamination at Sites 999 (Bralower et al., 1997) and 1260 (Erbacher, Moser, Malone, et al., 2004) and the appearance of a unique low-oxygen assemblage of benthic foraminifers at all Leg 198 sites (Kahio et al., submitted [N1]). Still, all Shatsky Rise PETM sediments are homogeneous and organic matter content is minimal, indicating that bottom waters did not become anoxic.

Estimated bottom water warming of ~6°C during the PETM (e.g., Kennett and Stott, 1991; Zachos et al., 2003) would also have lowered dissolved oxygen levels. Using the equation (Broecker and Peng, 1982)

$$O_2\ (\mu mol/kg) = 350 - 9T + 0.14T^2,$$

where

$T$ = temperature (°C),

and deepwater temperature estimates from ODP Site 865 (10° and 16°C pre-PETM and PETM, respectively) (Bralower et al., 1995), the decrease in deepwater dissolved oxygen content was from ~274 µmol/kg to ~242 µmol/kg. Dissolved $O_2$ in the modern western equatorial Pacific is ~260 µmol/kg (Broecker and Peng, 1982), similar to pre-PETM estimates. Unless ocean circulation was significantly different from the present causing lower Pacific $O_2$ levels, deepwater warming was insufficient to cause $O_2$ depletion. $O_2$ depletion resulting from $CH_4$ oxidation in the deep ocean may be responsible for pore water dysoxia in the absence of elevated productivity. Alternatively, increased pyrite contents may reflect highly condensed sections near the base of the PETM at the Shatsky Rise sites.

Pyrite precipitation at the PETM may alternatively be related to increased supply of Fe to the ocean. Increased chemical weathering on continents as a result of global warming would increase the Fe flux to the oceans. This is a viable explanation for the pyrite peak if Fe, not sulfate, was a limiting factor in pyrite precipitation. However, this alternative would cause increased pyrite throughout the warming interval, not just at the onset, as indicated in the PETM intervals on Shatsky Rise.

## CONCLUSIONS

The PETM was an abrupt climate shift ~55 m.y. ago associated with a host of biotic changes and a negative CIE in oceanic and continental reservoirs. Many of the postulated causes of the event involve introduction of a large amount of $CO_2$ or $CH_4$ into the ocean-atmosphere system and result in a rapid shoaling of the lysocline and CCD. This response can be tested with an examination of foraminiferal preservation and detailed counts of fragmentation, fish debris, and pyrite in conjunction with $CaCO_3$ content. Detailed analysis of foraminiferal preservational proxies (i.e., fragmentation, benthic/planktonic foraminiferal ratios, coarse fraction, and $CaCO_3$ content) from Shatsky Rise PETM sections and visual observations of foraminiferal preservation indicate that fragmentation most accurately mirrors foraminiferal preservation. $CaCO_3$ content and benthic/planktonic ratios also identify intervals of poorest visual preservation. Fragmentation, $CaCO_3$ content, and fish debris data indicate abrupt lysocline shoaling and dissolution of $CaCO_3$ within the sediment column (carbonate burn-down). Minimum lysocline shoaling is ~500 m in the tropical Pacific Ocean, significantly greater than model estimates assuming input of $CO_2$ or $CH_4$ in the deep Atlantic. Increases in pyrite at the basal lithologic contact indicate depleted $O_2$ in pore waters possibly due to $CH_4$ oxidation in the water column or an increase in Fe supply to the ocean.

## ACKNOWLEDGMENTS

Funding for this project came from Joint Oceanographic Institute, Inc.-U.S. Science Advisory Committee and the National Science Foundation (EAR-9814604 and EAR-0120727). The authors also wish to thank Debbie Thomas for technical assistance and Joe Carter, Drew Coleman, Jerry Dickens, Dick Kroon, and Micah Nicolo for reviews.

This research used samples and/or data provided by the Ocean Drilling Program (ODP). ODP is funded by the U.S. National Science Foundation (NSF) under management of Joint Oceanographic Institutions, Inc. (JOI).

## REFERENCES

Arrhenius, G., 1952. Sediment cores from the East Pacific. *In* Pettersson, H. (Ed.), *Rep. Swed. Deep-Sea Exped., 1947–1948,* 5:189–201.

Bains, S., Corfield, R.M., and Norris, R.D., 1999. Mechanisms of climate warming at the end of the Paleocene. *Science,* 285:724–727.

Berner, R.A., 1977. Sulfate reduction and the rate of deposition in marine sediments. *Earth Planet. Sci. Lett.,* 37:492–498.

Boersma, A., Premoli Silva, I., and Hallock, P., 1998. Trophic models for well-mixed and poorly mixed warm oceans across the Paleocene/Eocene epoch boundary. *In* Aubry, M.P., Lucas, S.G., and Berggren, W.A. (Eds.), *Late Paleocene–Early Eocene Biotic and Climatic Events in the Marine and Terrestrial Records:* New York (Columbia Univ. Press), 204–213.

Bralower, T.J., 2002. Evidence for surface water oligotrophy during the Late Paleocene–Eocene Thermal Maximum: nannofossil assemblages data from Ocean Drilling Program Site 690, Maud Rise, Weddell Sea. *Paleoceanography,* 17(2):1–12:10.1029/2001PA000662

Bralower, T.J., Premoli Silva, I., and Malone, M.J., 2002. New evidence for abrupt climate change in the Cretaceous and Paleogene: an Ocean Drilling Program expedition to Shatsky Rise, Northwest Pacific. *Geol. Soc. Am. Today,* 12(11):4–10.

Bralower, T.J., Premoli Silva, I., Malone, M.J., et al., 2002. *Proc. ODP, Init. Repts.,* 198 [Online]. Available from World Wide Web: <http://www-odp.tamu.edu/publications/198_IR/198ir.htm.> [Cited 2005-10-31]

Bralower, T.J., Thomas, D.J., Zachos, J.C., Hirschmann, M.M., Röhl, U., Sigurdsson, H., Thomas, E., and Whitney, D.L., 1997. High-resolution records of the Late Paleocene Thermal Maximum and circum-Caribbean volcanism: is there a causal link? *Geology,* 25:963–966.

Bralower, T.J., Zachos, J.C., Thomas, E., Parrow, M., Paull, C.K., Kelly, D.C., Premoli Silva, I., Sliter, W.V., and Lohmann, K.C., 1995. Late Paleocene to Eocene paleoceanography of the equatorial Pacific Ocean: stable isotopes recorded at Ocean Drilling Program Site 865, Allison Guyot. *Paleoceanography,* 10(40):841–865.

Broecker, W.S., and Peng, T.-H., 1982. *Tracers in the Sea:* Palisades, NY (Eldigio Press).

Canudo, J.I., Keller, G., Molina, E., and Ortiz, N., 1995. Planktonic foraminiferal turnover and $\delta^{13}C$ isotopes across the Paleocene–Eocene transition at Caravaca and Zumaya, Spain. *Palaeogeogr., Palaeoclimatol., Palaeoecol.,* 114:75–100.

Colosimo, A.B., 2004. Evidence for lysocline shoaling and carbonate "burn down" at the Paleocene–Eocene Thermal Maximum on Shatsky Rise, ODP Leg 198 [M.S. thesis]. Univ. North Carolina, Chapel Hill.

Corliss, B.H., and Honjo, S., 1981. Dissolution of deep-sea benthonic foraminifera. *Micropaleontology,* 27:356–378.

Crouch, E.M., Heilmann-Clausen, C., Brinkhuis, H., Morgans, H.E.G., Rogers, K.M., Egger, H., and Schmitz, B., 2001. Global dinoflagellate event associated with the Late Paleocene Thermal Maximum. *Geology,* 29:315–318.

de Baar, H.J.W., and de Jong, J.T.M., 2001. Distributions, sources and sinks of iron in seawater. *In* Turner, D.R., and Hunger, K.A. (Eds.), *The Biogeochemistry of Iron in Seawater:* Indianapolis (Wiley).

Dickens, G.R., 2000. Methane oxidation during the Late Palaeocene Thermal Maximum. *Bull. Soc. Geol. Fr.,* 171:37–49.

Dickens, G.R., 2001. Carbon addition and removal during the Late Palaeocene Thermal Maximum: basic theory with a preliminary treatment of the isotope record at ODP Site 1051, Blake Nose. *In* Kroon, D., Norris, R.D., and Klaus, A. (Eds.), *Western North Atlantic Paleogene and Cretaceous Paleoceanography,* Spec. Publ.—Geol. Soc. London, 183:293–306.

Dickens, G.R., Castillo, M.M., and Walker, J.G.C., 1997. A blast of gas in the latest Paleocene: simulating first-order effects of massive dissociation of oceanic methane hydrate. *Geology,* 25(3):259–262.

Dickens, G.R., O'Neil, J.R., Rea, D.K., and Owen, R.M., 1995. Dissociation of oceanic methane hydrate as a cause of the carbon isotope excursion at the end of the Paleocene. *Paleoceanography,* 10:965–971.

Eldholm, O., and Thomas, E., 1993, Environmental impact of volcanic margin formation. *Earth Planet. Sci. Lett.,* 117:319–329.

Erbacher, J., Mosher, D.C., Malone, M.J., et al., 2004. *Proc. ODP, Init. Repts.,* 207 [Online]. Available from World Wide Web: <http://www-odp.tamu.edu/publications/207_IR/207ir.htm>. [Cited 2005-10-31]

Haug, G.H., and Tiedemann, R., 1998. Effect of the formation of the Isthmus of Panama on Atlantic Ocean thermohaline circulation. *Nature (London, U. K.),* 393:673–676.

Katz, M.E., Pak, D.K., Dickens, G.R., and Miller, K.G., 1999. The source and fate of massive carbon input during the Latest Paleocene Thermal Maximum. *Science,* 286:1531–1533.

Kelly, D.C., Bralower, T.J., and Zachos, J.C., 1998. Evolutionary consequences of the Latest Paleocene Thermal Maximum for tropical planktonic foraminifera. *Palaeogeogr., Palaeoclimatol., Palaeoecol.,* 141:139–161.

Kennett, J.P., and Stott, L.D., 1991. Abrupt deep-sea warming, paleoceanographic changes and benthic extinctions at the end of the Palaeocene. *Nature (London, U. K.),* 353:225–229.

Kent, D.V., Cramer, B.S., Lanci, L., Wang, D., Wright, J.D., and Van der Voo, R., 2003. A case for a comet impact trigger for the Paleocene/Eocene Thermal Maximum and carbon isotope excursion. *Earth Planet. Sci. Lett.,* 211:13–26.

Koch, P.L., Zachos, J.C., and Gingerich, P.D., 1992. Correlation between isotope records in marine and continental carbon reservoirs near the Palaeocene/Eocene boundary. *Nature (London, U. K.),* 358:319–322.

Kurtz, A.C., Kump, L.R., Arthur, M.A., Zachos, J.C., and Paytan, A., 2003. Early Cenozoic decoupling of the global carbon and sulfur cycles. *Paleoceanography,* 18:1090:10.1029/2003PA000908.

Kvenvolden, K.A., 1993. Gas hydrates: geological perspective and global change. *Rev. Geophys.,* 31:173–187.

Lerman, A., 1979. *Geochemical Processes: Water and Sediment Environments:* New York (John Wiley and Sons).

Lipps, J.H., 1973. Test structure in foraminifera. *Ann. Rev. Microbiol.,* 27:471–488.

Lu, G., and Keller, G., 1993. The Paleocene–Eocene transition in the Antarctic Indian Ocean: inference from planktonic foraminifera. *Mar. Micropaleontol.,* 21:101–142.

Lyle, M., Wilson, P.A., Janecek, T.R., et al., 2002. *Proc. ODP, Init. Repts.,* 199 [Online]. Available from World Wide Web: <http://www-odp.tamu.edu/publications/199_IR/199ir.htm>. [Cited 2005-10-31]

Maas, M.C., Anthony, M.R.L., Gingerich, P.D., Gunnell, G.F., and Krause, D.W., 1995. Mammalian genetic diversity and turnover in the late Paleocene and early Eocene of the Bighorn and Crazy Mountain basins, Wyoming and Montana (USA). *Palaeogeogr., Palaeoclimatol., Palaeoecol.,* 115:181–207.

Müller, P.J., and Suess, E., 1979. Productivity, sedimentation rate, and sedimentary organic matter in the oceans, I. Organic carbon preservation. *Deep-Sea Res. Part A,* 26:1347–1362.

Norris, R.D., Kroon, D., Klaus, A., et al., 1998. *Proc. ODP, Init. Repts.,* 171B: College Station, TX (Ocean Drilling Program).

Schlanger, S.O., and Douglas, R.G., 1974. The pelagic ooze-chalk-limestone transition and its implication for marine stratigraphy. *In* Hsü, K.J., and Jenkyns, H.C. (Eds.), *Pelagic Sediments: On Land and Under the Sea.* Spec. Publ.—Int. Assoc. Sedimentol., 1:117–148.

Schmitz, B., Speijer, R.P., and Aubry, M.-P., 1996. Latest Paleocene benthic extinction event on the southern Tethyan shelf (Egypt): foraminiferal stable isotopic ($\delta^{13}C$, $\delta^{18}O$) records. *Geology,* 24:347–350.

Stoll, H.M., and Bains, S., 2003. Coccolith Sr/Ca records of productivity during the Paleocene–Eocene Thermal Maximum from the Weddell Sea. *Paleoceanography,* 18(2):10.1029/2002PA000875.

Svenson, H., Planke, S., Malthe-Sørenssen, A., Jamtveit, B., Myklebust, R., Eidem, T.R., and Rey, S.S., 2004. Release of methane from a volcanic basin as a mechanism for initial Eocene global warming. *Nature*, 429:542–545.

Thierstein, H.R., and Roth, P.H., 1991. Stable isotopic and carbonate cyclicity in Lower Cretaceous deep-sea sediments: dominance of diagenetic effects. *Mar. Geol.,* 97:1–34.

Thomas, D.J., Bralower, T.J., and Zachos, J.C., 1999. New evidence for subtropical warming during the Late Paleocene Thermal Maximum: stable isotopes from Deep Sea Drilling Project Site 527, Walvis Ridge. *Paleoceanography,* 14:561–570.

Thomas, D.J., Zachos, J.C., Bralower, T.J., Thomas, E., and Bohaty, S., 2002. Warming the fuel for the fire: evidence for the thermal dissociation of methane hydrate during the Paleocene–Eocene Thermal Maximum. *Geology,* 30:1067–1070.

Thomas, E., 1998. Biogeography of the late Paleocene benthic foraminiferal extinction. *In* Aubry, M.-P., Lucas, S.G., and Berggren, W.A. (Eds.), *Late Paleocene–Early Eocene Biotic and Climatic Events in the Marine and Terrestrial Records:* New York (Columbia Univ. Press), 214–243.

Thomas, E., and Shackleton, N., 1996. The Palaeocene–Eocene benthic foraminiferal extinction and stable isotope anomalies. *In* Knox, R.W.O'B., Corfield, R.M., and Dunay, R.E. (Eds.), *Correlation of the Early Paleogene in Northwest Europe*. Geol. Soc. Spec. Publ., 101:401–441.

Thomas, E., Zachos, J.C., and Bralower, T.J., 2000. Ice-free to glacial world transition as recorded by benthic foraminifera. *In* Huber, B.T., MacLeod, K.G., and Wing, S.L. (Eds.), *Warm Climates in Earth History:* Cambridge (Cambridge Univ. Press), 132–160.

Thomas, D. J., Bralower, T. J., and Jones, C. E., 2003. Neodymium isotopic reconstruction of late Paleocene–early Eocene thermohaline circulation. *Earth Planet. Sci. Lett.,* 209:309–322.

Walker, J.C.G., and Kasting, J.F., 1992. Effects of fuel and forest conservation on future levels of atmospheric carbon dioxide. *Global Planet. Change,* 5:151–189.

Zachos, J.C., Kroon, D., Blum, P., et al., 2004. *Proc. ODP, Init. Repts.,* 208 [Online]. Available from World Wide Web: <http://www-odp.tamu.edu/publications/208_IR/208ir.htm>. [Cited 2005-10-31]

Zachos, J.C., Röhl, U., Schellenberg, S.A., Sluijs, A., Hodell, D.A., Kelly, D.C., Thomas, E., Nicolo, M., Raffi, I., Lourens, L.J., McCarren, H., and Kroon, D., 2005. Rapid acidification of the ocean during the Paleocene–Eocene Thermal Maximum. *Science,* 308:1611–1616.

Zachos, J.C., Wara, M.W., Bohaty, S., Delaney, M.L., Petrizzo, M.R., Brill, A., Bralower, T.J., and Premoli Silva, I., 2003. A transient rise in tropical sea surface temperature during the Paleocene–Eocene Thermal Maximum. *Science,* 302:10.1126/science.1090110.

**Figure F1.** Bathymetric map of Shatsky Rise showing location of sites investigated. Sites 1209, 1210, 1211, and 1212 are on the Southern High (Bralower, Premoli Silva, Malone, et al., 2002).

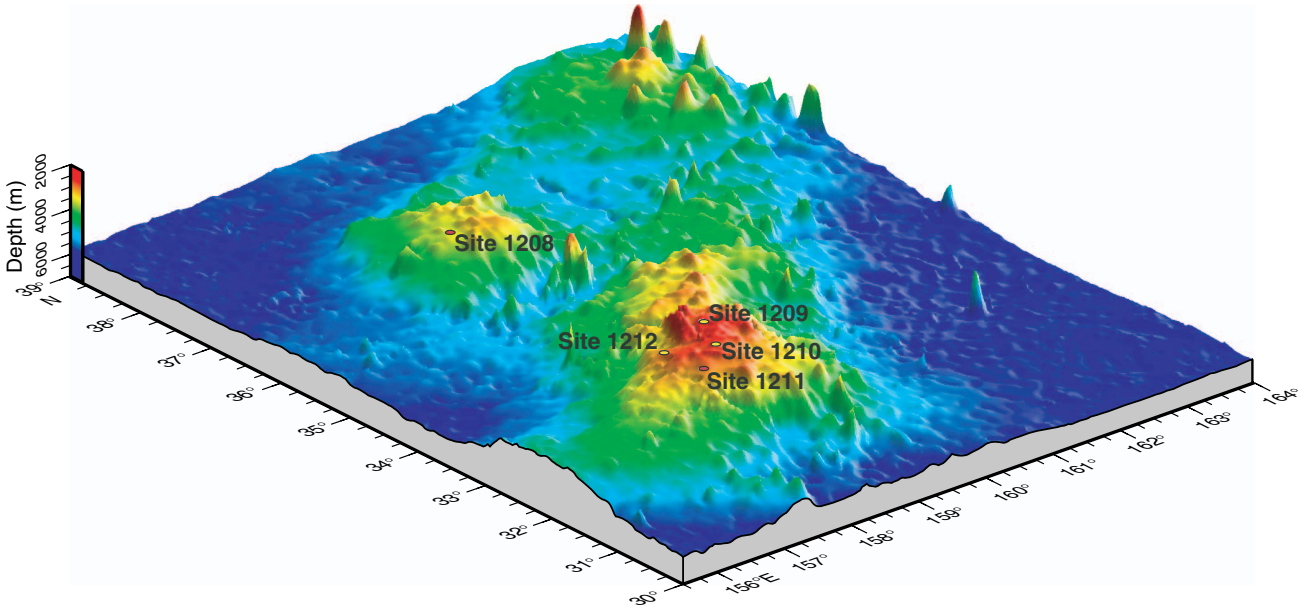

**Figure F2.** PETM on Shatsky Rise. Onset of event is recognized by major changes in lithology, carbonate content, foraminiferal preservation, and the presence of bulk sediment CIE. PETM at Site 1208 is recognized by preservational change and confirmed by bulk sediment carbon isotope stratigraphy. Sites are organized by present (and paleo) water depth.

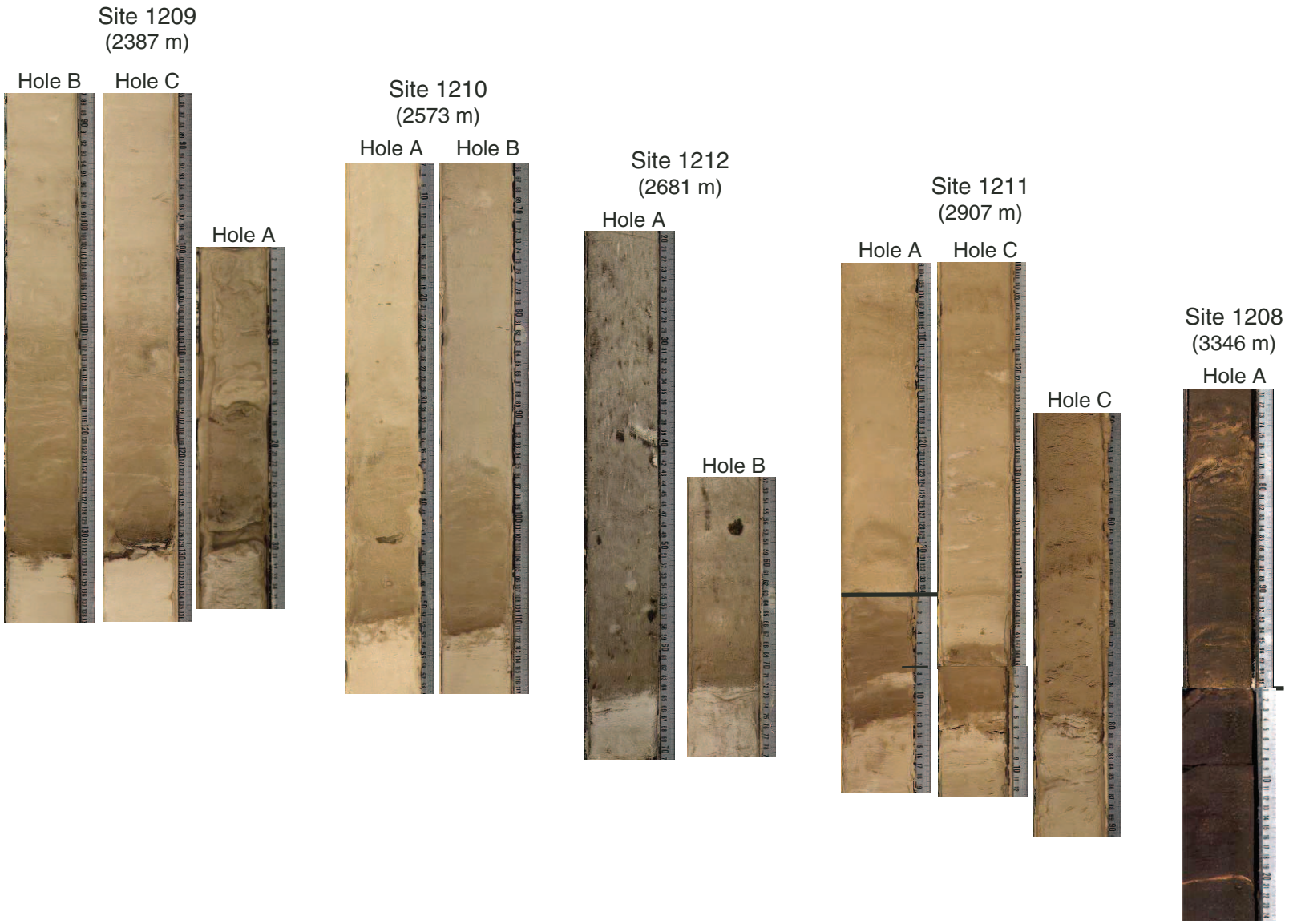

**Figure F3.** Plot of >38- and >63-µm size fractions vs. depth in Hole 1210B. The >38- and >63-µm fractions show similar stratigraphic trends.

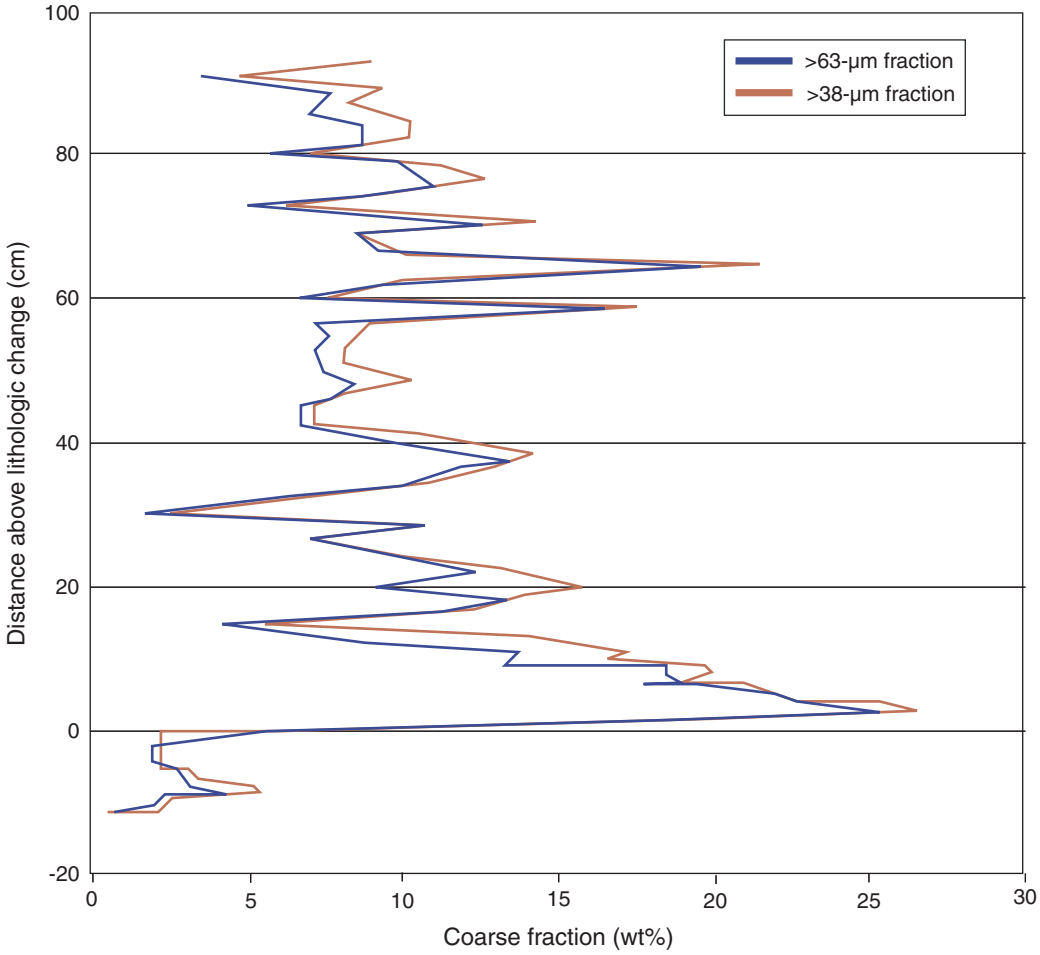

**Figure F4.** Histogram showing replicate counts of 300 specimens in three different samples to determine internal consistency. Results show reproducibility = ±10%. Percent whole and percent total fragments refer to planktonic foraminifers.

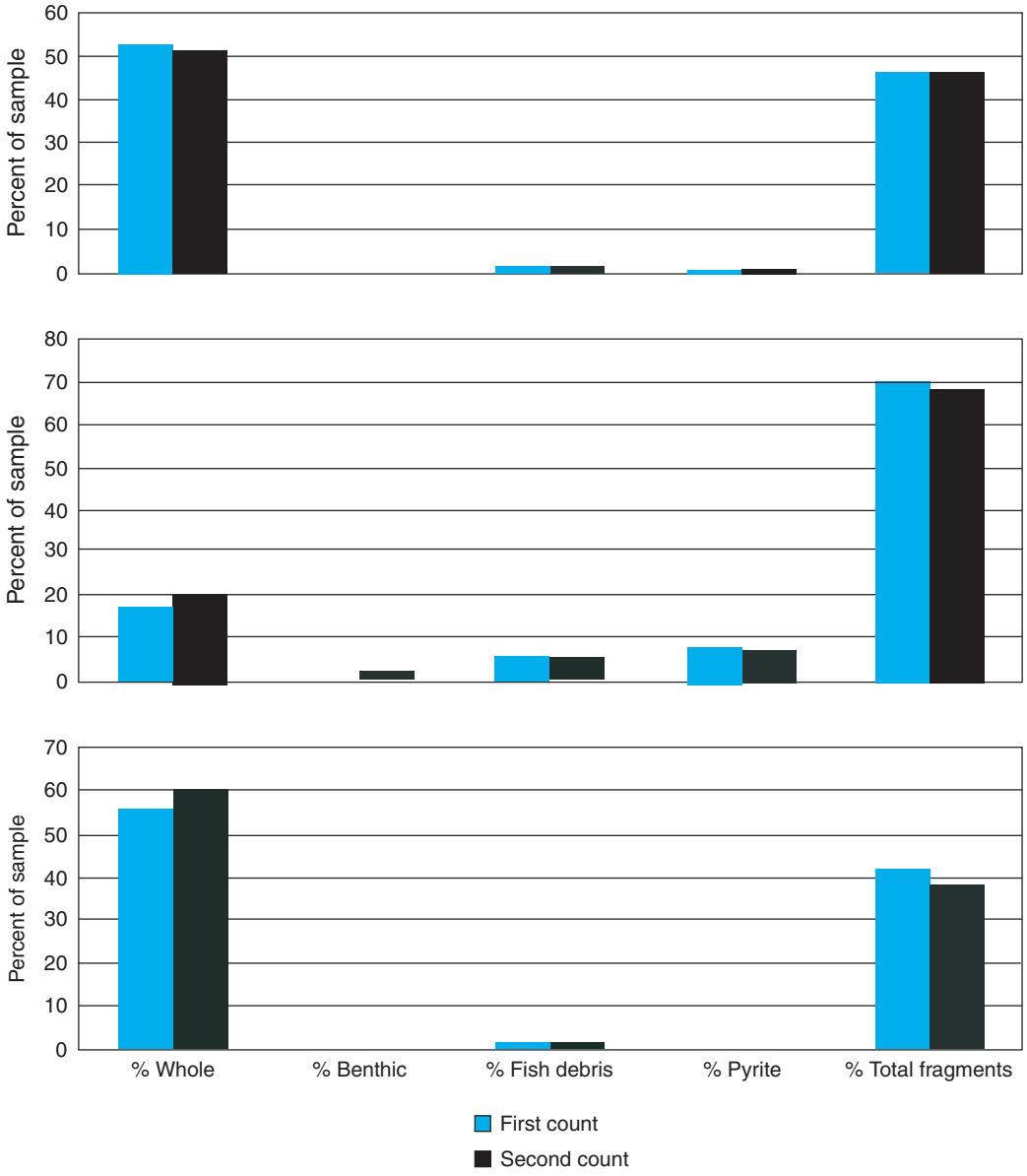

**Figure F5.** Bulk $\delta^{13}C$ values, coarse fraction, $CaCO_3$, fragmentation (planktonic foraminifers), benthic/planktonic (B/P) foraminiferal ratios, pyrite, and fish debris in samples across the Paleocene/Eocene Thermal Maximum (PETM) in Hole 1209B. Photograph is of the working half of the core that has been offset downward during sampling by 2.5 cm with respect to the archive half (see Fig. F2, p. 18). 0 cm = base of CIE.

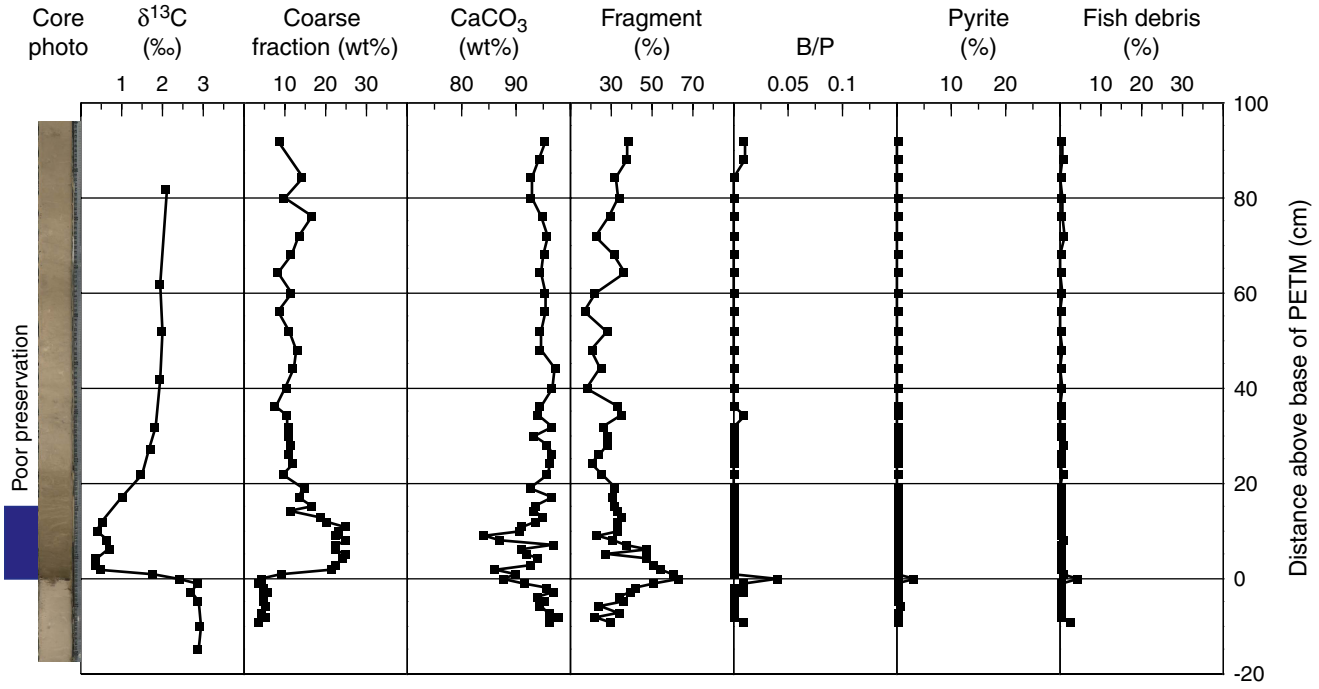

**Figure F6.** Bulk $\delta^{13}C$ values, coarse fraction, $CaCO_3$, fragmentation (planktonic foraminifers), benthic/planktonic (B/P) foraminiferal ratios, pyrite, and fish debris in samples across the Paleocene/Eocene Thermal Maximum (PETM) in Hole 1210B. 0 cm = base of CIE.

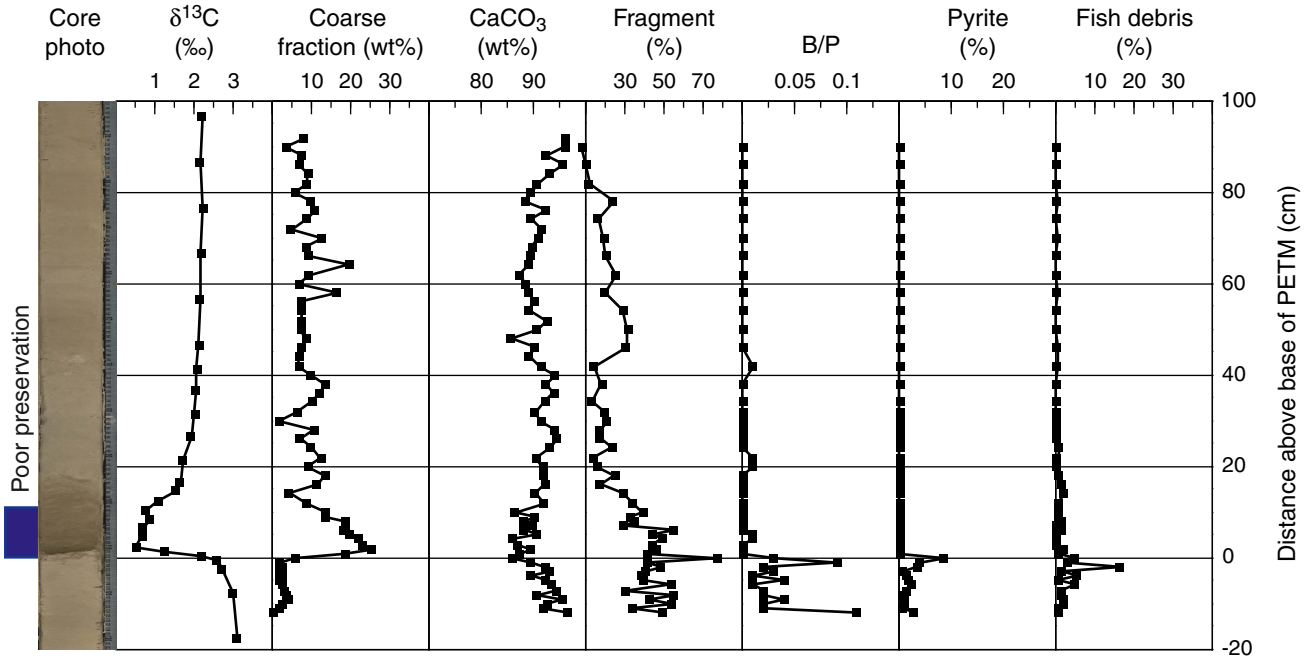

**Figure F7.** Bulk $\delta^{13}C$ values (from Hole 1212A), coarse fraction, $CaCO_3$, fragmentation (planktonic foraminifers), benthic/planktonic (B/P) foraminiferal ratios, pyrite, and fish debris in samples across the Paleocene/Eocene Thermal Maximum (PETM) in Hole 1212B. 0 cm = base of CIE determined in Hole 1212A.

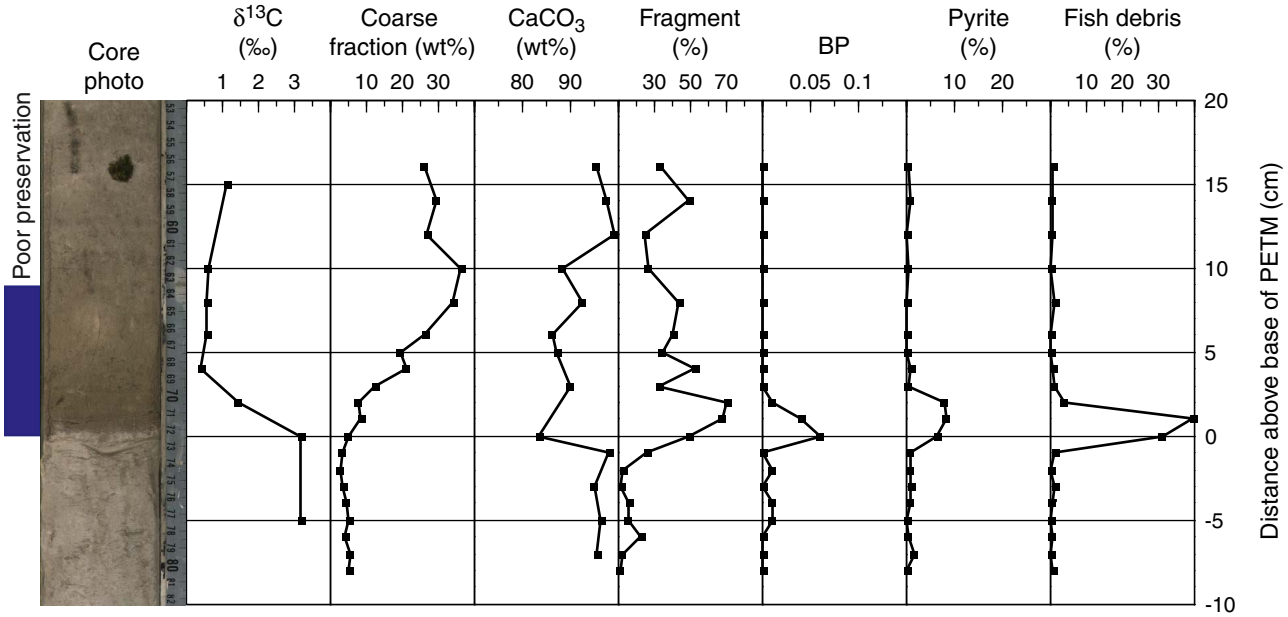

**Figure F8.** Bulk $\delta^{13}C$ values, coarse fraction, $CaCO_3$, fragmentation (planktonic foraminifers), benthic/planktonic (B/P) foraminiferal ratios, pyrite, and fish debris in samples across the Paleocene/Eocene Thermal Maximum (PETM) in Hole 1211C. 0 cm = base of CIE.

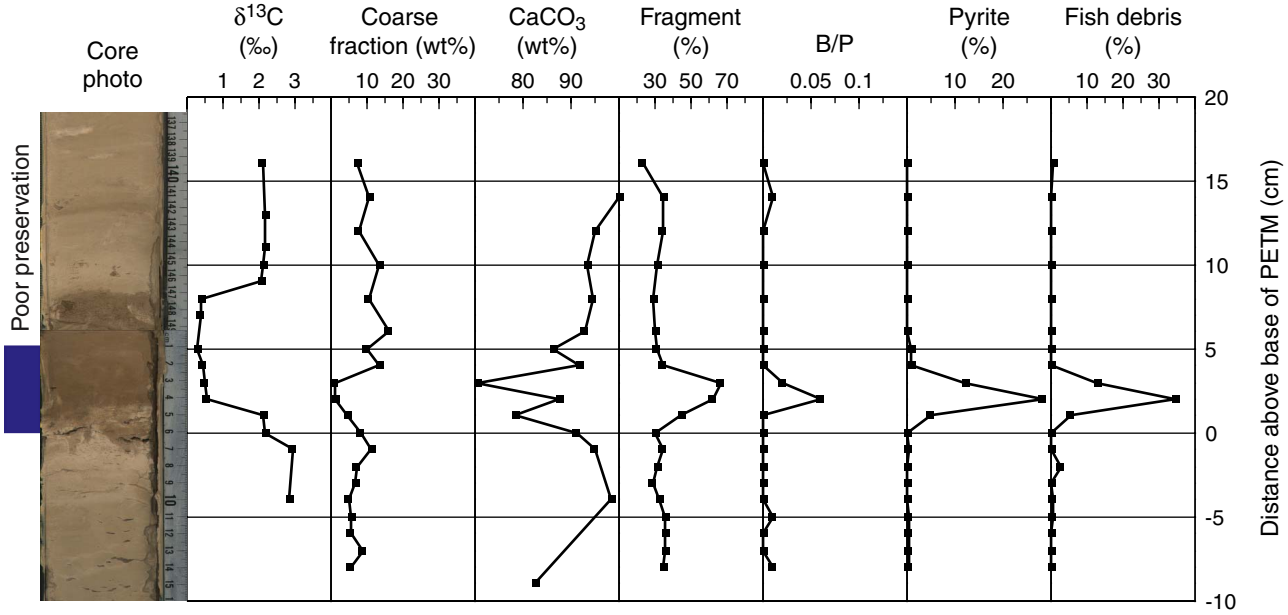

**Table T1.** Compositional data for PETM, Hole 1209B.

| Core, section, interval (cm) | Depth (mbsf) | Above PETM (cm) | Benthic foraminifers (*N*) | B/P ratio | $CaCO_3$ (wt%) | Coarse fraction (wt%) | Whole planktonic foraminifers (%) | Benthic foraminifers (%) | Fish debris (%) | Pyrite (%) | Planktonic foraminifer fragmentation (%) |
|---|---|---|---|---|---|---|---|---|---|---|---|
| 198-1209B- | | | | | | | | | | | |
| 22H-1, 43 | 195.53 | 92 | 2 | 0.01 | 95.33 | 8.37 | 61.39 | 0.63 | 0.32 | 0.00 | 37.78 |
| 22H-1, 45 | 195.55 | 88 | 1 | 0.01 | 94.17 | | 62.30 | 0.32 | 0.64 | 0.00 | 37.30 |
| 22H-1, 51 | 195.61 | 84 | 0 | 0.00 | 92.75 | 14.36 | 68.09 | 0.00 | 0.00 | 0.00 | 31.91 |
| 22H-1, 55 | 195.65 | 80 | 1 | 0.00 | 92.75 | 9.79 | 65.76 | 0.30 | 0.30 | 0.00 | 33.74 |
| 22H-1, 59 | 195.69 | 76 | 1 | 0.00 | 94.67 | 16.32 | 70.32 | 0.25 | 0.25 | 0.00 | 29.25 |
| 22H-1, 63 | 195.73 | 72 | 1 | 0.00 | 95.58 | 13.33 | 76.63 | 0.30 | 0.89 | 0.00 | 22.19 |
| 22H-1, 67 | 195.77 | 68 | 0 | 0.00 | 95.08 | 11.44 | 69.00 | 0.00 | 0.00 | 0.00 | 31.00 |
| 22H-1, 71 | 195.81 | 64 | 0 | 0.00 | 94.42 | 8.13 | 63.58 | 0.00 | 0.00 | 0.00 | 36.42 |
| 22H-1, 75 | 195.85 | 60 | 0 | 0.00 | 95.33 | 11.35 | 77.83 | 0.00 | 0.22 | 0.00 | 21.96 |
| 22H-1, 79 | 195.89 | 56 | 0 | 0.00 | 95.17 | 8.41 | 83.39 | 0.00 | 0.00 | 0.00 | 16.61 |
| 22H-1, 83 | 195.93 | 52 | 0 | 0.00 | 94.33 | 10.92 | 72.31 | 0.00 | 0.00 | 0.00 | 27.69 |
| 22H-1, 87 | 195.97 | 48 | 0 | 0.00 | 94.50 | 12.72 | 79.80 | 0.00 | 0.26 | 0.00 | 19.95 |
| 22H-1, 91 | 196.01 | 44 | 1 | 0.00 | 97.08 | 12.13 | 75.00 | 0.33 | 0.00 | 0.00 | 24.67 |
| 22H-1, 95 | 196.05 | 40 | 0 | 0.00 | 96.42 | 10.12 | 68.34 | 0.00 | 0.30 | 0.00 | 18.05 |
| 22H-1, 99 | 196.09 | 36 | 0 | 0.00 | 94.42 | 7.44 | 67.05 | 0.00 | 0.00 | 0.00 | 32.95 |
| 22H-1, 101 | 196.11 | 34 | 1 | 0.01 | 94.08 | 10.25 | 65.36 | 0.33 | 0.00 | 0.00 | 34.31 |
| 22H-1, 103 | 196.13 | 32 | 0 | 0.00 | 96.50 | 10.66 | 74.23 | 0.00 | 0.00 | 0.00 | 25.77 |
| 22H-1, 105 | 196.15 | 30 | 1 | 0.00 | 93.17 | 10.76 | 71.43 | 0.32 | 0.00 | 0.00 | 28.25 |
| 22H-1, 107 | 196.17 | 28 | 0 | 0.00 | 95.67 | 11.22 | 71.47 | 0.00 | 0.51 | 0.26 | 27.98 |
| 22H-1, 109 | 196.19 | 26 | 0 | 0.00 | 96.42 | 10.75 | 76.16 | 0.00 | 0.00 | 0.00 | 23.84 |
| 22H-1, 111 | 196.21 | 24 | 0 | 0.00 | 96.17 | 11.89 | 79.94 | 0.00 | 0.00 | 0.00 | 20.06 |
| 22H-1, 113 | 196.23 | 22 | 0 | 0.00 | 95.58 | 9.6 | 74.37 | 0.00 | 0.63 | 0.00 | 25.16 |
| 22H-1, 116 | 196.26 | 19 | 0 | 0.00 | 92.50 | 14.58 | 68.18 | 0.00 | 0.00 | 0.00 | 31.82 |
| 22H-1, 118 | 196.28 | 17 | 0 | 0.00 | 96.58 | 13.29 | 69.37 | 0.00 | 0.00 | 0.00 | 30.63 |
| 22H-1, 120 | 196.3 | 15 | 0 | 0.00 | 93.42 | 16.4 | 68.15 | 0.00 | 0.00 | 0.00 | 31.85 |
| 22H-1, 121 | 196.31 | 14 | 0 | 0.00 | 93.17 | 11.22 | 67.55 | 0.00 | 0.00 | 0.00 | 32.45 |
| 22H-1, 122 | 196.32 | 13 | 0 | 0.00 | 94.83 | 18.57 | 65.13 | 0.00 | 0.00 | 0.00 | 34.87 |
| 22H-1, 123 | 196.33 | 12 | 0 | 0.00 | 93.33 | 20.3 | 67.41 | 0.00 | 0.00 | 0.00 | 32.59 |
| 22H-1, 124 | 196.34 | 11 | 0 | 0.00 | 91.17 | 24.4 | 67.03 | 0.00 | 0.00 | 0.00 | 32.97 |
| 22H-1, 125 | 196.35 | 10 | 0 | 0.00 | 90.58 | 22.87 | 66.95 | 0.00 | 0.00 | 0.00 | 33.05 |
| 22H-1, 126 | 196.36 | 9 | 0 | 0.00 | 84.00 | 22.47 | 77.00 | 0.00 | 0.00 | 0.00 | 23.00 |
| 22H-1, 127 | 196.37 | 8 | 0 | 0.00 | 86.83 | 24.84 | 68.67 | 0.00 | 0.63 | 0.00 | 30.89 |
| 22H-1, 128 | 196.38 | 7 | 0 | 0.00 | 96.67 | 22.47 | 63.35 | 0.00 | 0.00 | 0.00 | 36.65 |
| 22H-1, 129 | 196.39 | 6 | 0 | 0.00 | 90.83 | 22.42 | 52.40 | 0.00 | 0.00 | 0.00 | 47.60 |
| 22H-1, 130 | 196.4 | 5 | 0 | 0.00 | 91.75 | 24.65 | 72.29 | 0.00 | 0.32 | 0.00 | 27.39 |
| 22H-1, 131 | 196.41 | 4 | 0 | 0.00 | 94.00 | 24 | 52.22 | 0.00 | 0.32 | 0.00 | 47.62 |
| 22H-1, 132 | 196.42 | 3 | 0 | 0.00 | 92.50 | 22.6 | 49.59 | 0.00 | 0.27 | 0.00 | 50.27 |
| 22H-1, 133 | 196.43 | 2 | 0 | 0.00 | 86.00 | 21.09 | 45.85 | 0.00 | 0.33 | 0.33 | 53.85 |
| 22H-1, 134 | 196.44 | 1 | 0 | 0.00 | 89.75 | 8.84 | 39.40 | 0.00 | 0.66 | 0.00 | 60.33 |
| 22H-1, 135 | 196.45 | 0 | 4 | 0.04 | 87.50 | 4.02 | 33.12 | 1.29 | 4.18 | 3.22 | 62.85 |
| 22H-1, 136 | 196.46 | –1 | 1 | 0.01 | 91.33 | 3.69 | 48.87 | 0.32 | 0.32 | 0.00 | 50.65 |
| 22H-1, 137 | 196.47 | –2 | 0 | 0.00 | 95.75 | 4.82 | 62.13 | 0.00 | 0.33 | 0.00 | 41.00 |
| 22H-1, 138 | 196.48 | –3 | 1 | 0.01 | 96.67 | 5.53 | 60.57 | 0.32 | 0.00 | 0.00 | 39.12 |
| 22H-1, 139 | 196.49 | –4 | 0 | 0.00 | 93.83 | 4.47 | 66.56 | 0.00 | 0.00 | 0.00 | 33.44 |
| 22H-1, 140 | 196.5 | –5 | 0 | 0.00 | 95.33 | 4.91 | 63.96 | 0.00 | 0.00 | 0.32 | 35.71 |
| 22H-1, 141 | 196.51 | –6 | 1 | 0.00 | 94.50 | 4.99 | 75.08 | 0.33 | 0.00 | 0.66 | 23.93 |
| 22H-1, 142 | 196.52 | –7 | 0 | 0.00 | 95.92 | 3.88 | 66.67 | 0.00 | 0.00 | 0.00 | 33.33 |
| 22H-1, 143 | 196.53 | –8 | 1 | 0.00 | 97.83 | 5.06 | 78.73 | 0.32 | 0.00 | 0.00 | 21.59 |
| 22H-1, 144 | 196.54 | –9 | 2 | 0.01 | 95.92 | 3.68 | 68.21 | 0.66 | 2.32 | 0.00 | 28.81 |

Note: PETM = Paleocene/Eocene Thermal Maximum, B/P = benthic/planktonic foraminifer.

**Table T2.** Compositional data for PETM, Hole 1210B.

| Core, section, interval (cm) | Depth (mbsf) | Above PETM (cm) | Benthic foraminifers (*N*) | B/P ratio | $CaCO_3$ (wt%) | Coarse fraction (wt%) | Whole planktonic foraminifers (%) | Fish debris (%) | Pyrite (%) | Planktonic foraminifer fragmentation (%) |
|---|---|---|---|---|---|---|---|---|---|---|
| 198-1210B. | | | | | | | | | | |
| 20H-3, 20-21 | 183.4 | 92 | | | 96.08 | 8.07 | | | | |
| 20H-3, 22-23 | 183.42 | 90 | 1 | 0.00 | 95.92 | 3.53 | 76.25 | 0.00 | 0.00 | 0.00 |
| 20H-3, 24-25 | 183.44 | 88 | | | 92.42 | 7.61 | | | | |
| 20H-3, 26-27 | 183.46 | 86 | 0 | 0.00 | 95.75 | 6.74 | 86.80 | 0.00 | 0.00 | 0.00 |
| 20H-3, 28-29 | 183.48 | 84 | | | 93.25 | 8.86 | | | | |
| 20H-3, 30-31 | 183.5 | 82 | 0 | 0.00 | 90.75 | 8.79 | 81.11 | 0.00 | 0.00 | 0.00 |
| 20H-3, 32-33 | 183.52 | 80 | | | 89.42 | 5.55 | | | | |
| 20H-3, 34-35 | 183.54 | 78 | 0 | 0.00 | 88.33 | 9.88 | 75.48 | 0.32 | 0.00 | 24.28 |
| 20H-3, 36-37 | 183.56 | 76 | | | 92.33 | 10.90 | | | | |
| 20H-3, 38-39 | 183.58 | 74 | 0 | 0.00 | 89.33 | 8.79 | 81.82 | 0.00 | 0.00 | 0.00 |
| 20H-3, 40-41 | 183.6 | 72 | | | 91.58 | 4.85 | | | | |
| 20H-3, 42-43 | 183.62 | 70 | 0 | 0.00 | 90.83 | 12.52 | 80.51 | 0.26 | 0.00 | 19.28 |
| 20H-3, 44-45 | 183.64 | 68 | | | 89.58 | 8.39 | | | | |
| 20H-3, 46-47 | 183.66 | 66 | 0 | 0.00 | 89.42 | 9.06 | 79.66 | 0.00 | 0.00 | 0.00 |
| 20H-3, 48-49 | 183.68 | 64 | | | 89.00 | 19.45 | | | | |
| 20H-3, 50-51 | 183.7 | 62 | 0 | 0.00 | 87.08 | 9.30 | 80.23 | 0.00 | 0.00 | 0.00 |
| 20H-3, 52-53 | 183.72 | 60 | | | 88.67 | 6.67 | | | | |
| 20H-3, 54-55 | 183.74 | 58 | 0 | 0.00 | 89.08 | 16.46 | 80.06 | 0.30 | 0.00 | 19.70 |
| 20H-3, 56-57 | 183.76 | 56 | | | 90.00 | 7.23 | | | | |
| 20H-3, 58-59 | 183.78 | 54 | 0 | 0.00 | 88.92 | 7.67 | 74.93 | 0.00 | 0.00 | 0.00 |
| 20H-3, 60-61 | 183.8 | 52 | | | 92.58 | 7.23 | | | | |
| 20H-3, 62-63 | 183.82 | 50 | 0 | 0.00 | 90.67 | 7.26 | 71.84 | 0.00 | 0.00 | 0.00 |
| 20H-3, 64-65 | 183.84 | 48 | | | 85.58 | 8.36 | | | | |
| 20H-3, 66-67 | 183.86 | 46 | 0 | 0.00 | 90.33 | 7.50 | 65.70 | 0.36 | 0.00 | 30.43 |
| 20H-3, 68-69 | 183.88 | 44 | | | 89.00 | 6.65 | | | | |
| 20H-3, 70-71 | 183.9 | 42 | 3 | 0.01 | 91.33 | 6.72 | 84.86 | 0.32 | 0.00 | 13.92 |
| 20H-3, 72-73 | 183.92 | 40 | | | 94.08 | 9.85 | | | | |
| 20H-3, 74-75 | 183.94 | 38 | 0 | 0.00 | 92.25 | 13.30 | 82.30 | 0.00 | 0.00 | 17.70 |
| 20H-3, 76-77 | 183.96 | 36 | | | 93.75 | 12.08 | | | | |
| 20H-3, 78-79 | 183.98 | 34 | 0 | 0.00 | 92.08 | 10.18 | 84.95 | 0.00 | 0.00 | 12.85 |
| 20H-3, 80-81 | 184 | 32 | 0 | 0.00 | 90.25 | 6.25 | 80.52 | 0.00 | 0.00 | 19.48 |
| 20H-3, 82-83 | 184.02 | 30 | 1 | 0.00 | 91.25 | 1.69 | 78.06 | 0.00 | 0.00 | 20.97 |
| 20H-3, 84-85 | 184.04 | 28 | 1 | 0.00 | 94.08 | 10.66 | 82.21 | 0.31 | 0.00 | 17.23 |
| 20H-3, 86-87 | 184.06 | 26 | 0 | 0.00 | 94.42 | 7.04 | 82.77 | 0.00 | 0.00 | 17.23 |
| 20H-3, 88-89 | 184.08 | 24 | 0 | 0.00 | 93.08 | 9.91 | 75.69 | 0.92 | 0.00 | 23.60 |
| 20H-3, 90-91 | 184.1 | 22 | 3 | 0.01 | 90.42 | 12.30 | 78.33 | 0.33 | 0.00 | 13.71 |
| 20H-3, 92-93 | 184.12 | 20 | 3 | 0.01 | 91.75 | 8.98 | 83.37 | 0.00 | 0.00 | 15.90 |
| 20H-3, 94-95 | 184.14 | 18 | 0 | 0.00 | 91.67 | 13.32 | 74.70 | 0.72 | 0.00 | 24.76 |
| 20H-3, 96-97 | 184.16 | 16 | 0 | 0.00 | 92.08 | 11.32 | 81.37 | 1.24 | 0.00 | 17.61 |
| 20H-3, 98-99 | 184.18 | 14 | 1 | 0.00 | 90.33 | 4.30 | 69.28 | 1.96 | 0.00 | 29.00 |
| 20H-3, 100-101 | 184.2 | 12 | 1 | 0.00 | 92.00 | 8.66 | 66.01 | 0.65 | 0.00 | 33.88 |
| 20H-3, 102-103 | 184.22 | 10 | 0 | 0.00 | 86.50 | 13.72 | 60.76 | 0.63 | 0.00 | 38.85 |
| 20H-3, 103-104 | 184.23 | 9 | 1 | 0.00 | 90.33 | 13.44 | 66.98 | 0.63 | 0.00 | 32.28 |
| 20H-3, 104-105 | 184.24 | 8 | 0 | 0.00 | 88.17 | 18.35 | 63.80 | 1.48 | 0.00 | 35.24 |
| 20H-3, 105-106 | 184.25 | 7 | 0 | 0.00 | 89.75 | 18.72 | 70.00 | 0.29 | 0.29 | 29.60 |
| 20H-3, 106-107 | 184.26 | 6 | 0 | 0.00 | 88.25 | 17.75 | 44.10 | 1.40 | 0.00 | 55.27 |
| 20H-3, 107-108 | 184.27 | 5 | 1 | 0.01 | 90.67 | 19.45 | 55.69 | 0.29 | 0.00 | 43.86 |
| 20H-3, 108-109 | 184.28 | 4 | 1 | 0.01 | 86.17 | 22.14 | 50.28 | 0.28 | 0.00 | 49.30 |
| 20H-3, 109-110 | 184.29 | 3 | 0 | 0.00 | 87.00 | 22.77 | 56.68 | 0.00 | 0.00 | 43.32 |
| 20H-3, 110-111 | 184.3 | 2 | 0 | 0.00 | 89.42 | 25.33 | 52.49 | 1.66 | 0.24 | 46.49 |
| 20H-3, 111-112 | 184.31 | 1 | 0 | 0.00 | 87.33 | 18.46 | 58.25 | 1.01 | 0.00 | 41.16 |
| 20H-3, 112-113 | 184.32 | 0 | 7 | 0.03 | 85.83 | 5.60 | 19.52 | 4.86 | 8.53 | 76.82 |
| 20H-3, 113-114 | 184.33 | –1 | 15 | 0.09 | 89.50 | 1.95 | 50.00 | 2.85 | 4.11 | 41.16 |
| 20H-3, 114-115 | 184.34 | –2 | 2 | 0.02 | 92.08 | 2.50 | 40.59 | 16.50 | 3.30 | 48.56 |
| 20H-3, 115-116 | 184.35 | –3 | 5 | 0.03 | 93.17 | 1.95 | 56.95 | 1.32 | 0.66 | 40.48 |
| 20H-3, 116-117 | 184.36 | –4 | 1 | 0.01 | 89.42 | 2.20 | 57.24 | 5.26 | 1.32 | 38.38 |
| 20H-3, 117-118 | 184.37 | –5 | 9 | 0.04 | 92.42 | 1.92 | 57.14 | 0.56 | 1.96 | 38.79 |
| 20H-3, 118-119 | 184.38 | –6 | 2 | 0.01 | 93.33 | 2.62 | 42.60 | 4.83 | 2.11 | 53.57 |
| 20H-3, 119-120 | 184.39 | –7 | 4 | 0.02 | 94.17 | 3.15 | 66.56 | 1.29 | 1.29 | 30.36 |
| 20H-3, 120-121 | 184.4 | –8 | 3 | 0.02 | 90.67 | 3.33 | 43.12 | 1.35 | 0.45 | 55.40 |
| 20H-3, 121-122 | 184.41 | –9 | 6 | 0.04 | 95.50 | 4.17 | 54.31 | 1.92 | 0.96 | 42.11 |
| 20H-3, 122-123 | 184.42 | –10 | 4 | 0.02 | 92.50 | 2.30 | 44.04 | 1.70 | 0.97 | 53.75 |
| 20H-3, 123-124 | 184.43 | –11 | 4 | 0.02 | 91.75 | 1.87 | 64.49 | 0.62 | 0.62 | 33.54 |
| 20H-3, 124-125 | 184.44 | –12 | 14 | 0.11 | 96.42 | 0.46 | 43.58 | 1.01 | 2.70 | 49.82 |

Note: PETM = Paleocene/Eocene Thermal Maximum, B/P = benthic/planktonic foraminifer.

**Table T3.** Compositional data for PETM, Hole 1212B.

| Core, section, interval (cm) | Depth (mbsf) | Above PETM (cm) | Benthic foraminifers (*N*) | B/P ratio | $CaCO_3$ (wt%) | Coarse fraction (wt%) | Whole planktonic foraminifers (%) | Fish debris (%) | Pyrite (%) | Planktonic foraminifer fragmentation (%) |
|---|---|---|---|---|---|---|---|---|---|---|
| 198-1212B- | | | | | | | | | | |
| 9H-5, 56–57 | 79.76 | 16 | 0 | 0.00 | 95.25 | 25.77 | 66.33 | 0.67 | 0.33 | 33.00 |
| 9H-5, 58–59 | 79.78 | 14 | 0 | 0.00 | 97.33 | 29.32 | 50.23 | 0.45 | 0.68 | 49.20 |
| 9H-5, 60–61 | 79.8 | 12 | 1 | 0.00 | 99.08 | 26.84 | 74.76 | 0.32 | 0.00 | 24.68 |
| 9H-5, 62–63 | 79.82 | 10 | 0 | 0.00 | 88.17 | 36.13 | 55.40 | 0.00 | 0.28 | 26.21 |
| 9H-5, 64–65 | 79.84 | 8 | 0 | 0.00 | 92.42 | 33.92 | 55.70 | 1.30 | 0.00 | 43.56 |
| 9H-5, 66–67 | 79.86 | 6 | 0 | 0.00 | 86.17 | 26.23 | 59.81 | 0.00 | 0.00 | 40.19 |
| 9H-5, 67–68 | 79.87 | 5 | 0 | 0.00 | 87.08 | 19.13 | 66.04 | 0.00 | 0.00 | 33.96 |
| 9H-5, 68–69 | 79.88 | 4 | 0 | 0.00 | | 20.98 | 46.18 | 0.64 | 0.96 | 52.43 |
| 9H-5, 69–70 | 79.89 | 3 | 1 | 0.00 | 89.92 | 12.31 | 66.36 | 0.91 | 0.30 | 32.52 |
| 9H-5, 70–71 | 79.9 | 2 | 1 | 0.01 | | 7.63 | 26.38 | 3.68 | 7.67 | 69.90 |
| 9H-5, 71–72 | 79.91 | 1 | 5 | 0.04 | | 8.37 | 16.21 | 39.65 | 8.25 | 67.50 |
| 9H-5, 72–73 | 79.92 | 0 | 15 | 0.06 | 83.33 | 4.88 | 29.96 | 30.96 | 6.24 | 49.30 |
| 9H-5, 73–74 | 79.93 | –1 | 1 | 0.00 | 98.00 | 3.16 | 72.79 | 1.31 | 0.66 | 25.42 |
| 9H-5, 74–75 | 79.94 | –2 | 4 | 0.01 | | 2.53 | 85.67 | 0.00 | 0.64 | 12.50 |
| 9H-5, 75–76 | 79.95 | –3 | 1 | 0.00 | 94.92 | 3.41 | 86.50 | 1.23 | 0.92 | 11.29 |
| 9H-5, 76–77 | 79.96 | –4 | 3 | 0.01 | | 4.16 | 82.48 | 0.32 | 0.64 | 15.76 |
| 9H-5, 77–78 | 79.97 | –5 | 2 | 0.01 | 96.33 | 5.16 | 83.71 | 0.00 | 0.00 | 15.31 |
| 9H-5, 78–79 | 79.98 | –6 | 1 | 0.00 | | 4.01 | 76.80 | 0.33 | 0.33 | 22.37 |
| 9H-5, 79–80 | 79.99 | –7 | 1 | 0.00 | 95.50 | 5.24 | 85.89 | 0.00 | 1.53 | 11.84 |
| 9H-5, 80–81 | 80 | –8 | 1 | 0.00 | | 5.16 | 88.43 | 0.76 | 0.15 | 10.70 |

Note: PETM = Paleocene/Eocene Thermal Maximum, B/P = benthic/planktonic foraminifer.

**Table T4.** Compositional data for PETM, Hole 1211C.

| Core, section, interval (cm) | Depth (mbsf) | Above PETM (cm) | B/P ratio | $CaCO_3$ (%) | Coarse fraction (%) | Whole planktonic foraminifers (%) | Benthic foraminifers (%) | Fish debris (%) | Pyrite (%) | Planktonic foraminifer fragmentation (%) |
|---|---|---|---|---|---|---|---|---|---|---|
| 198-1211C- | | | | | | | | | | |
| 13H-2, 139 | 114.7 | 16 | 0.00 | | 7.33 | 70.23 | 0.00 | 0.65 | 0.00 | 22.80 |
| 13H-2, 141 | 114.72 | 14 | 0.01 | 100.00 | 10.66 | 65.24 | 0.57 | 0.00 | 0.00 | 34.38 |
| 13H-2, 143 | 114.74 | 12 | 0.00 | 95.00 | 7.54 | 66.22 | 0.00 | 0.00 | 0.00 | 33.78 |
| 13H-2, 145 | 114.76 | 10 | 0.00 | 93.42 | 13.46 | 68.99 | 0.00 | 0.00 | 0.00 | 31.01 |
| 13H-2, 147 | 114.78 | 8 | 0.00 | 94.50 | 10.45 | 71.15 | 0.00 | 0.00 | 0.00 | 28.85 |
| 13H-3, 0 | 114.8 | 6 | 0.00 | 92.75 | 16.01 | 69.78 | 0.00 | 0.00 | 0.00 | 30.22 |
| 13H-3, 1 | 114.81 | 5 | 0.00 | 86.33 | 9.76 | 68.33 | 0.00 | 0.00 | 0.96 | 30.71 |
| 13H-3, 2 | 114.82 | 4 | 0.00 | 91.75 | 13.51 | 65.30 | 0.00 | 0.00 | 0.95 | 34.08 |
| 13H-3, 3 | 114.83 | 3 | 0.02 | 70.42 | 0.86 | 24.46 | 2.42 | 12.90 | 12.10 | 66.30 |
| 13H-3, 4 | 114.84 | 2 | 0.06 | 87.50 | 1.07 | 8.47 | 5.76 | 34.58 | 28.14 | 61.82 |
| 13H-3, 5 | 114.85 | 1 | 0.00 | 78.33 | 4.64 | 49.69 | 0.31 | 5.25 | 4.94 | 44.48 |
| 13H-3, 6 | 114.86 | 0 | 0.00 | 91.08 | 8.22 | 69.66 | 0.00 | 0.00 | 0.00 | 30.34 |
| 13H-3, 7 | 114.87 | –1 | 0.00 | 94.75 | 11.23 | 65.48 | 0.00 | 0.00 | 0.32 | 34.30 |
| 13H-3, 8 | 114.88 | –2 | 0.00 | | 7.13 | 66.45 | 0.33 | 2.66 | 0.00 | 31.51 |
| 13H-3, 9 | 114.89 | –3 | 0.00 | | 6.77 | 71.75 | 0.00 | 0.00 | 0.00 | 28.25 |
| 13H-3, 10 | 114.9 | –4 | 0.00 | 98.42 | 4.87 | 67.30 | 0.31 | 0.31 | 0.00 | 32.28 |
| 13H-3, 11 | 114.91 | –5 | 0.01 | | 5.57 | 63.77 | 0.60 | 0.30 | 0.30 | 35.45 |
| 13H-3, 12 | 114.92 | –6 | 0.00 | | 5.43 | 63.94 | 0.25 | 0.00 | 0.33 | 35.66 |
| 13H-3, 13 | 114.93 | –7 | 0.00 | | 8.81 | 64.13 | 0.32 | 0.00 | 0.32 | 35.67 |
| 13H-3, 14 | 114.94 | –8 | 0.01 | | 5.40 | 64.50 | 0.60 | 0.00 | 0.26 | 34.72 |
| 13H-3, 15 | 114.95 | –9 | | 82.50 | | | | | | |

Note: PETM = Paleocene/Eocene Thermal Maximum, B/P = benthic/planktonic foraminifer.

**Plate P1.** Planktonic foraminifers from lower part of PETM, Sample 1209B-22H-1, 134 cm (+1 cm).

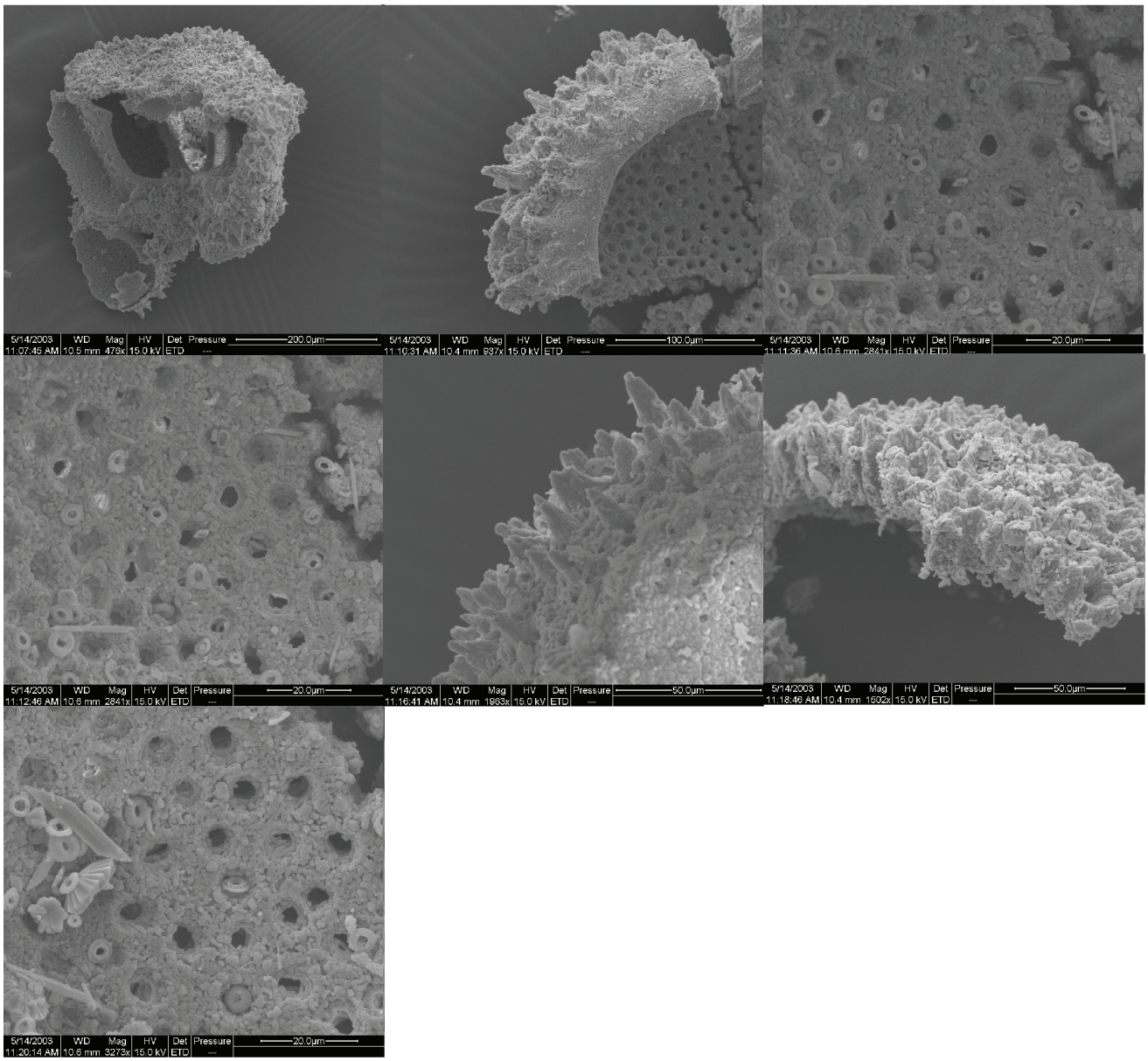

**Plate P2.** Planktonic foraminifers from lower part of PETM, Sample 1209B-22H-1, 133 cm (+2 cm).

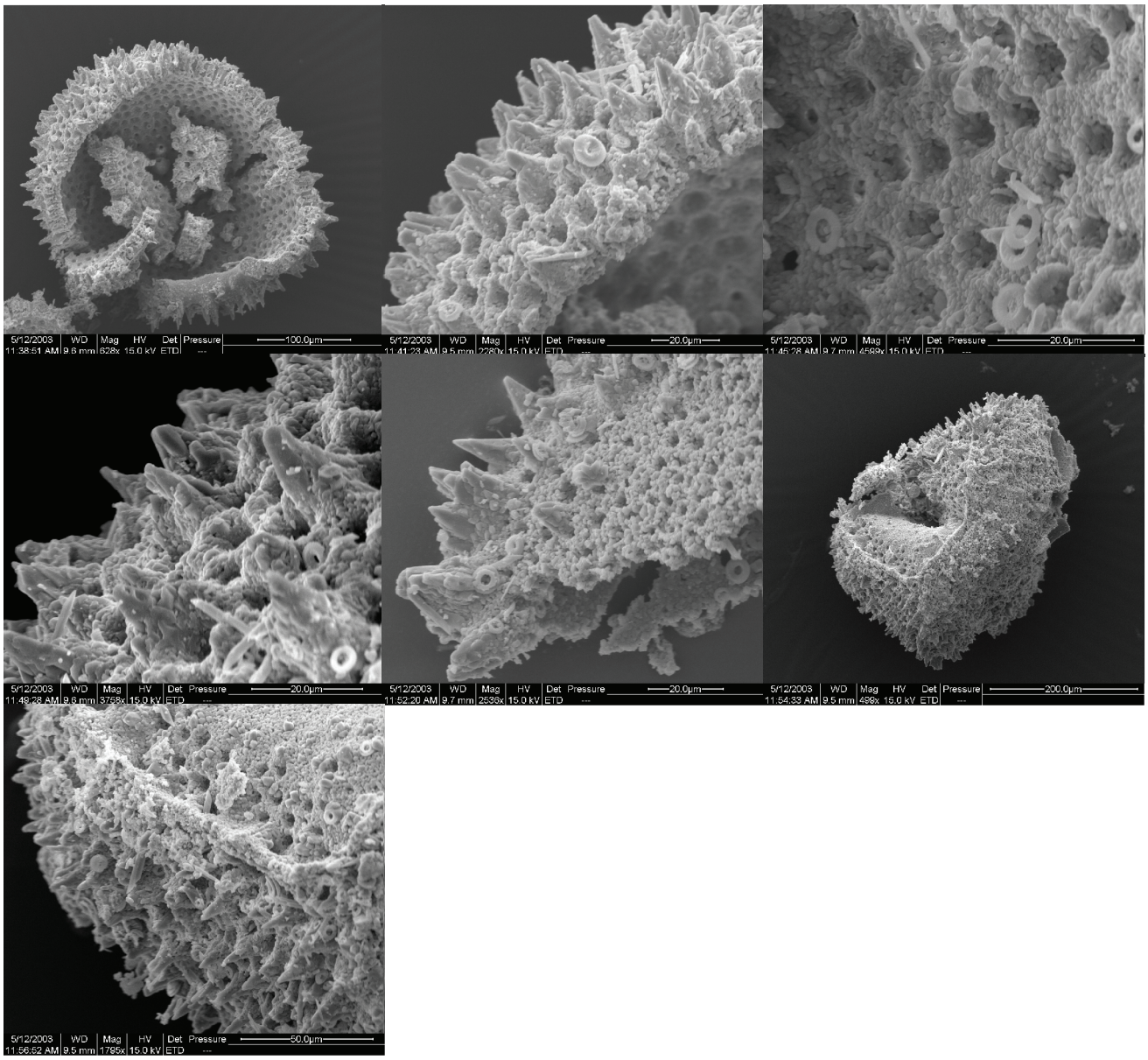

**Plate P3.** Planktonic foraminifers from lower part of PETM, Sample 1209B-22H-1, 132 cm (+3 cm).

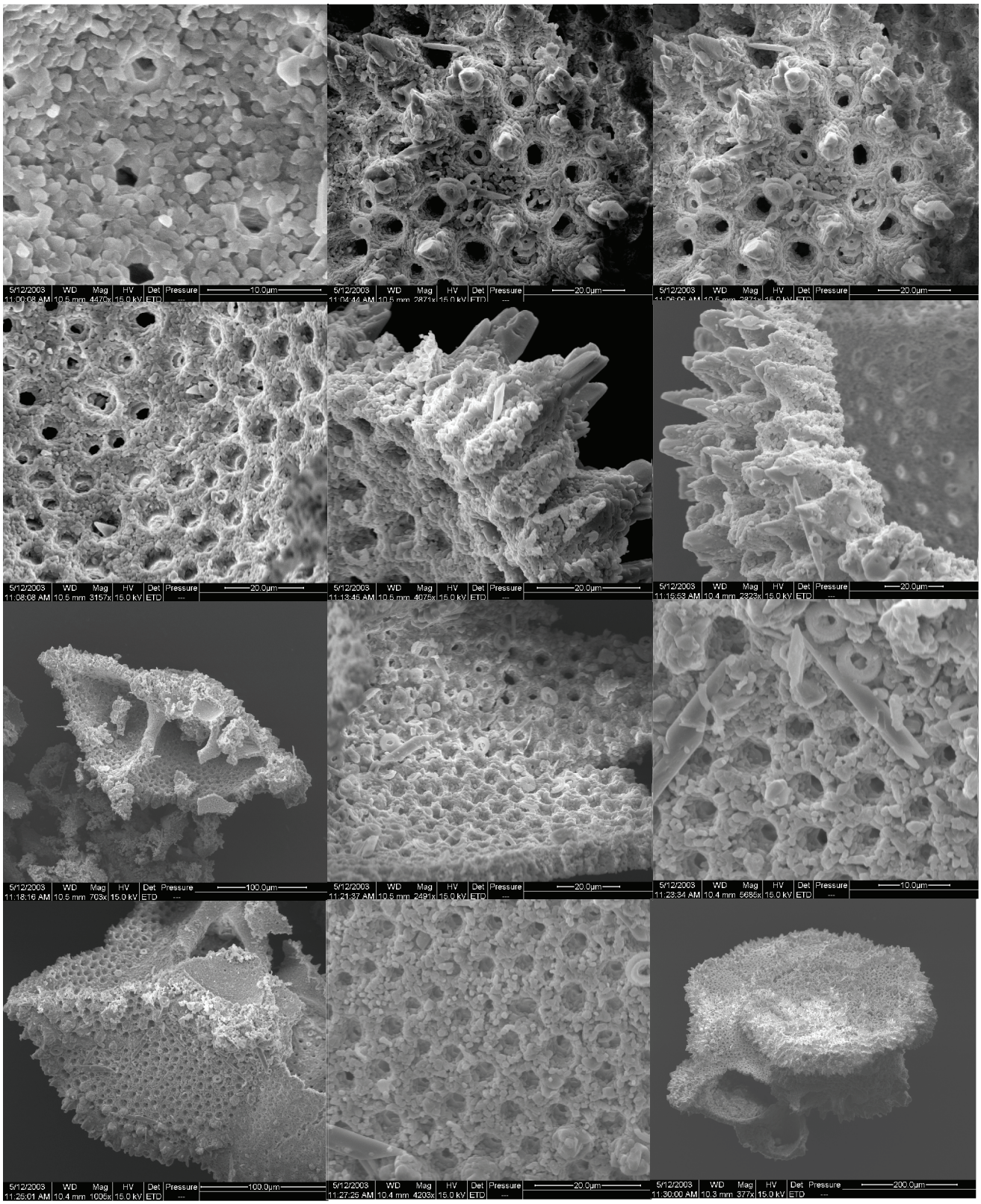

**Plate P4.** Planktonic foraminifers from lower part of PETM, Sample 1209B-22H-1, 131 cm (+4 cm).

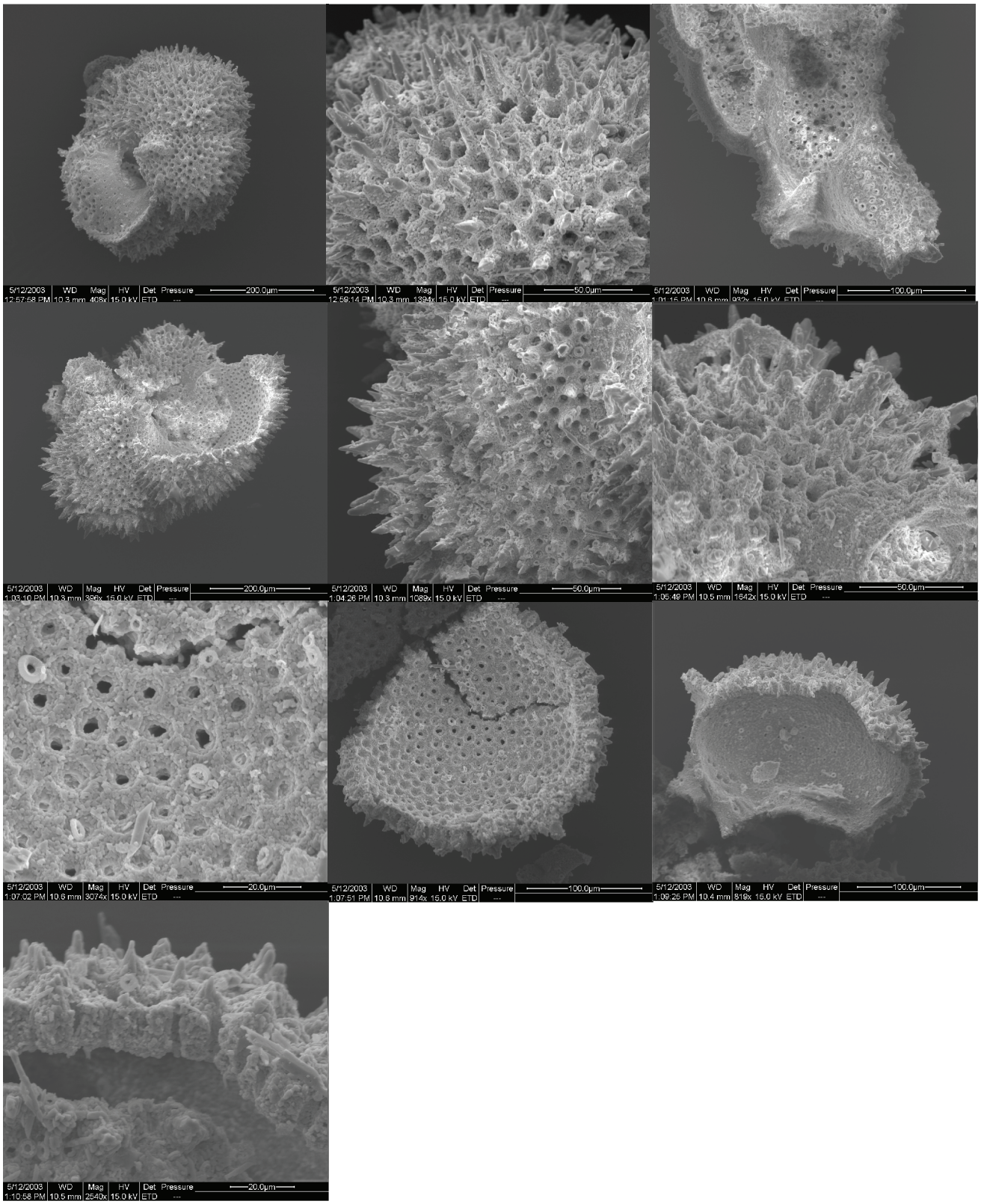

**Plate P5.** Planktonic foraminifers from lower part of PETM, Sample 1209B-22H-1, 130 cm (+5 cm).

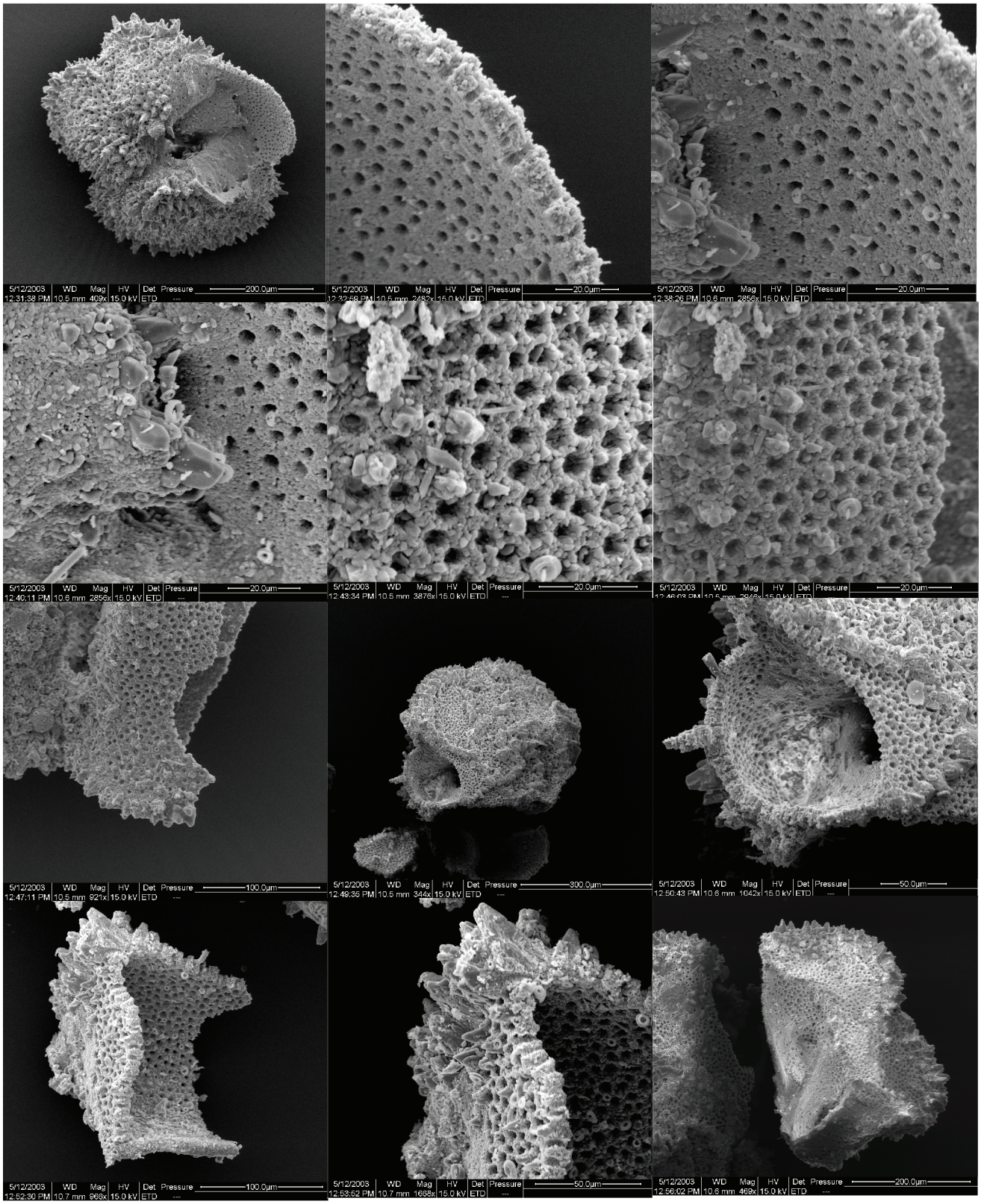

**Plate P6.** Planktonic foraminifers from lower part of PETM, Sample 1209B-22H-1, 129 cm (+6 cm).

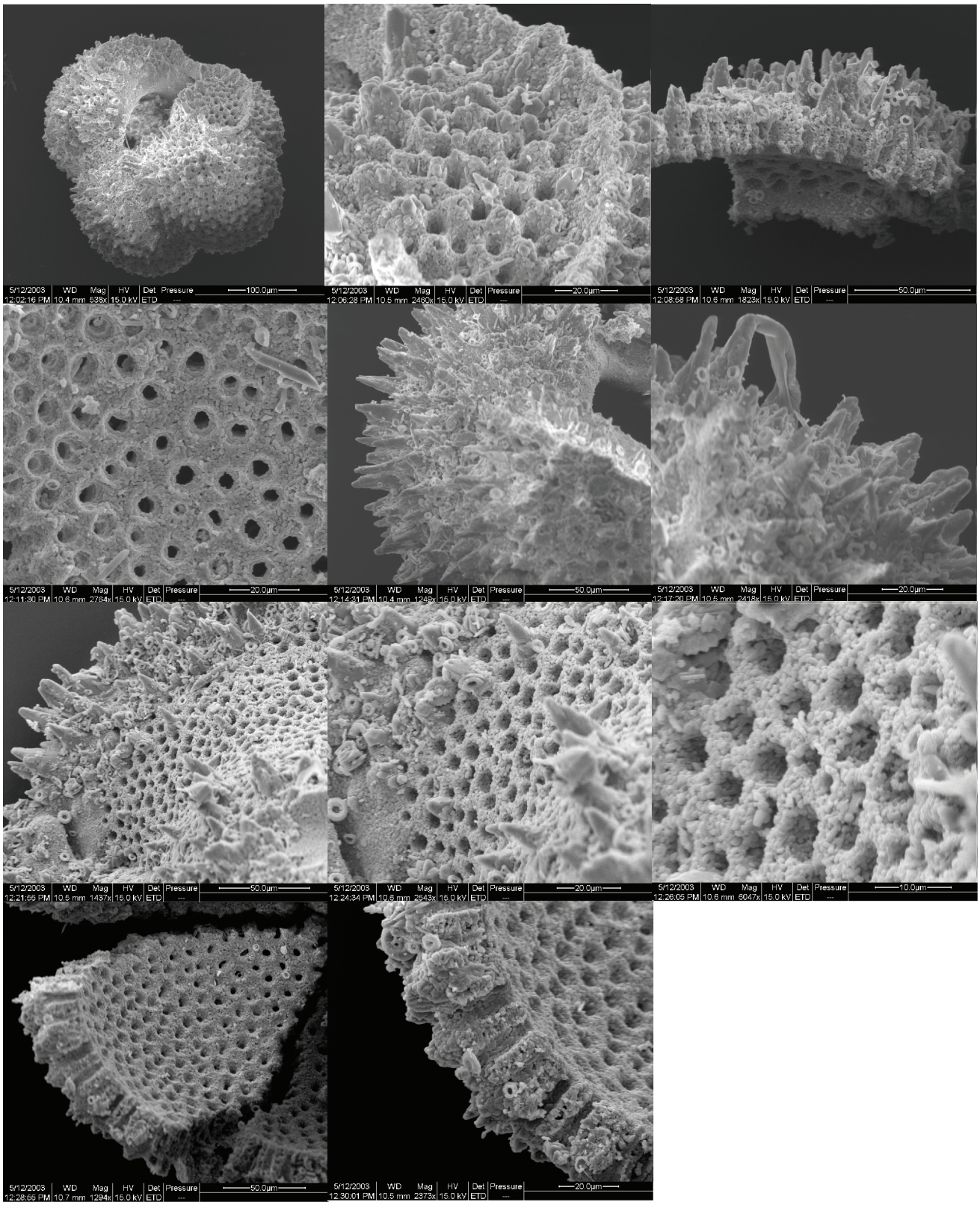

**Plate P7.** Planktonic foraminifers from lower part of PETM, Sample 1209B-22H-1, 128 cm (+7 cm).

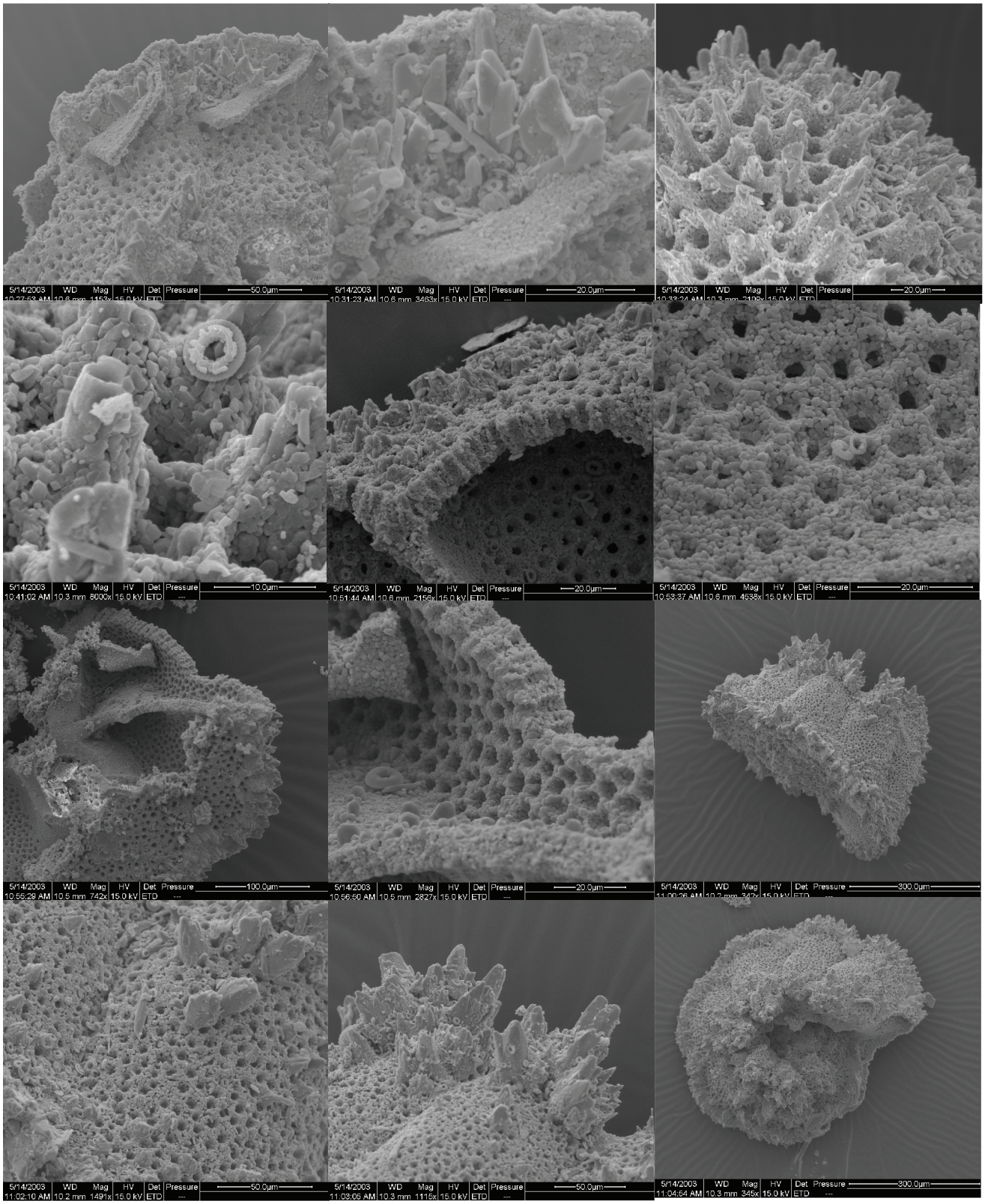

# CHAPTER NOTE*

**N1.** Kahio, K., Kotaro, T., Petrizzo, M.R., and Zachos, J.C., submitted. Anomalous shifts in tropical Pacific planktonic and benthic foraminiferal test size during the Paleocene-Eocene Thermal Maximum. *Palaeogeogr., Palaeoclimatol., Palaeoecol.*

*Dates reflect file corrections or revisions.